AGU PUBLICATIONS

JGR

Journal of Geophysical Research: Atmospheres

RESEARCH ARTICLE
10.1002/2017JD026704

Key Points:
- Demonstrates method for validating stratospheric temperature profile products using hyperspectral infrared radiance observations
- UCAR COSMIC RO and NASA AIRS v6 hyperspectral IR sounder temperatures and calculated radiances are compared
- AIRS L2 product found to contain unphysical structures in polar winters and a COSMIC warm bias found in the UTLS polar winters

Correspondence to:
M. L. Feltz,
michelle.feltz@ssec.wisc.edu

Citation:
Feltz, M. L., R. O. Knuteson, and H. E. Revercomb (2017), Assessment of COSMIC radio occultation and AIRS hyperspectral IR sounder temperature products in the stratosphere using observed radiances, *J. Geophys. Res. Atmos.*, *122*, 8593–8616, doi:10.1002/2017JD026704.

Received 27 FEB 2017
Accepted 19 JUL 2017
Accepted article online 7 AUG 2017
Published online 26 AUG 2017

Assessment of COSMIC radio occultation and AIRS hyperspectral IR sounder temperature products in the stratosphere using observed radiances

M. L. Feltz[1], R. O. Knuteson[1], and H. E. Revercomb[1]

[1]Space Science and Engineering Center, University of Wisconsin-Madison, Madison, Wisconsin, USA

Abstract Upper air temperature is defined as an essential climate variable by the World Meteorological Organization. Two remote sensing technologies being promoted for monitoring stratospheric temperatures are GPS radio occultation (RO) and spectrally resolved IR radiances. This study assesses RO and hyperspectral IR sounder derived temperature products within the stratosphere by comparing IR spectra calculated from GPS RO and IR sounder products to coincident IR observed radiances, which are used as a reference standard. RO dry temperatures from the University Corporation for Atmospheric Research (UCAR) Constellation Observing System for Meteorology, Ionosphere, and Climate (COSMIC) mission are compared to NASA Atmospheric Infrared Sounder (AIRS) retrievals using a previously developed profile-to-profile collocation method and vertical temperature averaging kernels. Brightness temperatures (BTs) are calculated for both COSMIC and AIRS temperature products and are then compared to coincident AIRS measurements. The COSMIC calculated minus AIRS measured BTs exceed the estimated 0.5 K measurement uncertainty for the winter time extratropics around 35 hPa. These differences are attributed to seasonal UCAR COSMIC biases. Unphysical vertical oscillations are seen in the AIRS L2 temperature product in austral winter Antarctic regions, and results imply a small AIRS tropical warm bias around ~35 hPa in the middle stratosphere.

1. Introduction

Upper air temperature is defined as an essential climate variable by the World Meteorological Organization [*Global Climate Observing System (GCOS)*, 2011]. A Global Climate Observing System (GCOS) report asserts that upper air temperatures are crucial for understanding changes in lower stratospheric water vapor, reconciling ozone trends from different instruments, validating climate models, and distinguishing between possible causes of climate change [*GCOS*, 2011], while *Huang et al.* [2016] recently demonstrated the role of the stratosphere in global climate prediction. Though a reliable, upper air temperature data set would clearly be an important asset to the scientific community, past work has shown the challenges of attaining one. According to the 2013 Intergovernmental Panel on Climate Change Working Group I AR5, "substantial disagreement exists among available estimates as to the rate of temperature changes," including its vertical structure [*Hartmann et al.*, 2013]. *Simmons et al.* [2014] concluded from a comparison of four major numerical weather prediction reanalyses that the middle stratosphere is the atmospheric region containing the largest temperature uncertainties. Likewise, *Thompson et al.* [2012], titled "The Mystery of Recent Stratospheric Temperature Trends," brought to light differences among climate model simulations and the available Stratospheric Sounding Unit (SSU), Microwave Sounding Unit (MSU), and radiosonde temperature data sets. Subsequently, recent, rigorous efforts have been put forth to reconcile these differences, document biases, and update trend estimates [e.g., *McLandress et al.*, 2015; *Nash and Saunders*, 2015; *Keckhut et al.*, 2015; *Wang et al.*, 2012a; *Zou et al.*, 2014; *Gaffen*, 1994; *He et al.*, 2009; *Sun et al.*, 2010, 2013; *Philipona et al.*, 2013; *Haimberger et al.*, 2008; *Funatsu et al.*, 2016]. However, the refined data sets still have limitations in their spatial and temporal coverage [*Seidel et al.*, 2011]—radiosondes lack sufficient global sampling, and they are often unable to reach altitudes above 50 hPa [*Sun et al.*, 2013; *Seidel et al.*, 2011], and SSUs were taken off the operational NOAA series in 2006. *Seidel et al.* [2016], which encapsulated the current status of agreement between the most recently processed MSU and SSU data sets, provided motivation for updated measurement technologies for the continuation of the stratospheric temperature climate data record.

Two relatively new remote sensing technologies being promoted for recording stratospheric temperatures are Global Positioning System (GPS) radio occultation (RO) and spectrally resolved infrared (IR) radiances

[*Goody et al*., 1995; *Anderson et al*., 2004; *Leroy et al*., 2006, 2008; *Steiner et al*., 2011; *GCOS*, 2011; *Huang et al*., 2010]. These technologies represent two climate benchmark measurements defined by the National Research Council (NRC) in the 2007 decadal survey [*Board and National Research Council*, 2007]. In response to the NRC report, NASA initiated the Climate Absolute Radiance and Refractivity Observatory (CLARREO) mission [*Wielicki et al*., 2013]. According to *Wielicki et al*. [2013],

"The first [benchmark measurement] is spectrally resolved infrared radiance (IR) emitted from Earth to space determined with an accuracy of 0.065 K (k = 2, or 95% confidence). The infrared spectra are traced to the SI standard for the kelvin. The second benchmark is the phase delay rate of the signal from the low-Earth-orbit Global Navigation Satellite System radio occultation system (GNSS-RO, or simply RO) occulted by the atmosphere, with an accuracy of 0.06% (k = 2) for a range of altitudes from 5 to 20 km in the atmosphere. The measurement is traced to the SI standard for the second."

These benchmark measurements, which have higher accuracy requirements than current operational instruments, would provide the ability to more accurately record upper air temperature. Though current hyperspectral IR and GPS RO measurements do not meet the CLARREO requirements, they already play an important role in the global space-based intercalibration system which plays a vital role in monitoring instrument accuracies [*Tobin et al*., 2006a, *Smith et al*., 2009; *Hilton et al*., 2012; *Tobin et al*., 2016; *Zou et al*., 2014; *Ho et al*., 2009; *Goldberg et al*., 2011].

As part of the preformulation phase of the CLARREO mission, a relative assessment of IR and RO derived temperature products was initiated which focused on the upper troposphere and lower stratosphere (UTLS) [*Feltz et al*., 2014a, 2014b]. In *Feltz et al*. [2014a], a matchup methodology was developed which minimizes spatiotemporal mismatch errors between temperature profiles derived from nadir-measured IR radiances and RO phase delays. This method, which accounts for the unique geometry and horizontal resolution of the RO profiles, was applied in *Feltz et al*. [2014b] to products from U.S. and European satellite centers and was refined in *Feltz et al*. [2017] to include vertical averaging kernels to degrade the higher vertical resolution RO profiles to match the inherent vertical resolution of the IR sounders. While this method provides the ability to compare derived temperatures from different instruments on common spatial and temporal scales, it is only able to provide a relative comparison since neither the IR nor RO derived temperature products are provided with rigorous absolute uncertainty estimates traceable to International System (SI) standards.

This study aims to provide an assessment of both IR and RO derived temperature products by extending the matchup method of *Feltz et al*. [2014a] to include the measured IR radiances as an absolute reference standard. Such a comparison to measured IR radiances, which has previously been illustrated in *Huang et al*. [2007] and *Bani Shahabadi et al*. [2016], avoids possible bias errors in the IR retrieval algorithms used to generate the IR temperature profiles. For this type of analysis, rigorous knowledge of the measured IR radiance uncertainty is a key component of a statistically meaningful result. Much work has been put into making absolute radiometric uncertainty assessments for IR emission spectrometers, including those on the ground, high-altitude aircraft, and satellites [*Revercomb et al*., 1988, 2003; *Knuteson et al*., 2004a, 2004b; *Tobin et al*., 2013]. Moreover, careful satellite-to-satellite and satellite-to-aircraft validation has been performed to characterize how each of the hyperspectral IR satellite sensors currently operate [*Tobin et al*., 2006b, 2006c; *Larar et al*., 2010; *Wang et al*., 2012b; *Han et al*., 2013; *Tobin et al*., 2013]. An overview of the ongoing international effort to provide traceability of observed infrared radiances to SI standards for the many sensors currently in orbit is given in *Goldberg et al*. [2011]. While only one hyperspectral IR sensor and one RO network are compared in this study, the outlined approach could be applied to any of the several hyperspectral IR and RO sensors and missions that are currently in orbit.

Specifically, this study compares temperature products from the NASA Atmospheric Infrared Sounder (AIRS) science team (version 6) and University Corporation for Atmospheric Research (UCAR) Constellation Observing System for Meteorology, Ionosphere, and Climate (COSMIC) RO products over the years 2007 through 2012. Comparisons are made in both temperature and radiance space with a focus on the UTLS. First, in section 4, comparisons of the entire, global data sets from AIRS Level 3 and COSMIC products are made for the 6 year time period. Next, section 5 addresses and minimizes the spatiotemporal mismatch errors that are present in the complete data set comparison of section 4. This is done by first applying the *Feltz et al*. [2014a] profile-to-profile matchup method to the AIRS L2 and COSMIC temperature products and then by

applying vertical temperature averaging kernels to the new matchup data set. This resulting data set contains minimized spatiotemporal mismatch errors yet still holds the same robust, statistical properties as the complete data set (from section 5) on zonally and monthly averaged time scales. Differences of the individual AIRS minus COSMIC matchup profiles are computed and used to calculate difference biases for various latitude zones and time scales. In section 6, to aid in the interpretation of the AIRS minus COSMIC matchup temperature bias from section 5, simulated radiances are calculated for both the AIRS and COSMIC temperatures for every matchup case. These simulated radiances are then compared to the corresponding AIRS measured radiances, which with their low radiometric uncertainty are used as a validation reference [*Tobin et al*., 2013]. Section 7 contains a discussion of the results, while section 8 provides conclusions. A brief review of the current state of IR and RO measurements is given in the next section.

2. Background

2.1. Hyperspectral IR Sounders

Hyperspectral infrared sounding of Earth's atmosphere, which has a history of over 30 years [*Smith et al*., 1983, 2009], has been successfully demonstrated under multiple satellite missions. Such missions include NASA's AIRS sensor that began operation in 2002 [*Parkinson*, 2003; *Aumann et al*., 2003; *Pagano et al*., 2003; *Strow et al*., 2003a], European Organisation for the Exploitation of Meteorological Satellites' Infrared Atmospheric Sounding Interferometer (IASI) series of instruments which were launched on the METOP-A platform in 2006 and on METOP-B in 2010 [*Hilton et al*., 2012; *Klaes et al*., 2007], and most recently NASA's Cross-track Infrared Sounder (CrIS) which was launched on the Suomi-National Polar-orbiting Partnership (NPP) satellite in preparation for the next U.S. Joint Polar Satellite System (JPSS) operational weather satellite series [Han *et al*., 2013*; Tobin et al*., 2013; *Strow et al*., 2013; *Nalli et al*., 2013; *Goldberg et al*., 2013]

Hyperspectral IR sounders have reduced radiometric uncertainty in comparison to earlier filter wheel radiometers [*Revercomb et al*., 1988; *Goody and Haskins*, 1998; *Tobin et al*., 2013]. However, even though their radiance measurements may have a high accuracy, their derived temperature products have uncertainties due to the ill-posed nature of the retrieval problem [*Rodgers*, 1976]. Past underlying purposes for retrieving temperatures have been for real-time operational forecasting, where speed of the retrieval scheme is a valued factor and a focus is set on accuracy within the lower atmosphere. Operating on polar orbiting satellites, IR sounders take measurements in large swaths that cover the globe twice daily. Retrievals from AIRS span the atmosphere from the surface up to 0.005 hPa [*Susskind et al*., 2003], though information at pressures less than ~1 hPa comes primarily from outside information—the AIRS L2 retrieval is not an IR-only product but is a combination of IR and microwave information. Stratospheric information comes from both the AIRS IR carbon dioxide absorption band and the Advanced Microwave Sounding Unit (AMSU) oxygen band. AIRS has a horizontal resolution of ~50 km, a vertical resolution that ranges from ~2.5 km in the troposphere to ~7 km in the stratosphere, has root-mean-square (RMS) requirements of 1 K for 1 km layers, and has uncertainty estimates of 1–2 K/km in the troposphere and 2–3 K/km above [*Divakarla et al*., 2006; *Maddy and Barnet*, 2008; *Olsen et al*., 2016]. Since the AIRS, CrIS, and IASI hyperspectral sounders were designed primarily for tropospheric sounding, only limited effort has been placed on stratospheric temperature sounding [*Hoffmann and Alexander*, 2009].

2.2. Radio Occultation

Radio occultation is a remote sensing, limb sounding technology that uses electromagnetic pulses sent out by the GPS constellation of satellites that are detected by receivers on low-Earth-orbiting satellites [*Kursinski et al*., 1997]. Stability of these observations is provided by the accuracy and reliability of the clocks used to monitor the occultations [*Leroy et al*., 2006; *Foelsche et al*., 2008, 2011b; *Steiner et al*., 2011]. The measured phase delays combined with knowledge of satellite positions are transformed into bending angles. Refractivity is then derived from the bending angles via an Abel transform and assumptions of horizontal symmetry, which can cause random and systematic errors in profiles with less verticality (i.e., larger incidence angles of the RO measurement rays with respect to the orbit plane of the receiving satellite, or azimuth angle) [*Foelsche et al*., 2011a]. Atmospheric refractivity, *N*, as a first order estimate for microwave wavelengths of the GPS signal is given by

$$N = 77.6\left(\frac{P}{T}\right) + 3.73\times10^5\left(\frac{P_w}{T^2}\right) + 4.03\times10^7\left(\frac{n_e}{f^2}\right) + 1.4W, \quad (1)$$

where P is pressure and P_w the water vapor partial pressure, T the temperature, n_e the electron number, f the transmitter frequency, and W the condensed water mass [*Kursinski et al.*, 1997]. The fourth term from the left is generally negligible, while the second moist atmospheric term is neglected for dry temperature retrievals. Dry temperature products do not properly represent the physical temperature in regions where the presence of water vapor is nonnegligible; however, since they are not dependent on background information, they can be more accurate than wet temperature products in the UTLS region [*Kursinski et al.*, 1997]. The ionospheric effect given to first order in the third term has been noted in the literature as an increasing concern for temperature retrieval accuracy and is corrected for by using the ionosphere's dispersive nature that affects the two GPS signals in different amounts [*Syndergaard*, 2000; *Mannucci et al.*, 2011, 2006; *Danzer et al.*, 2013]. While zeroth-order ionospheric contributions are removed from RO profiles at higher altitudes, residual errors can be amplified by the processing scheme and propagate downwards, thus affecting the temperature retrieval at lower altitudes [*Wee and Kuo*, 2014]. RO dry temperature is obtained via the ideal gas law after density is assumed proportional to the dry atmospheric contribution (the first term above), and pressure is derived via the hydrostatic equation.

Radio occultation can offer discrete profile measurements with a global distribution depending on the satellite orbit geometry. Derived temperature profiles have a vertical resolution of ~0.5 km in the troposphere to 2 km in the stratosphere and a horizontal resolution from 160 to 320 km [*Kursinski et al.*, 1997]. Various efforts have been put forth to model different error types of the retrieved profiles [*Foelsche et al.*, 2011a; *Steiner et al.*, 2013; *Alexander et al.*, 2014; *Scherllin-Pirscher et al.*, 2017], such as systematic errors that are introduced by the processing schemes of different data centers (also referred to as structural uncertainties) [*Ho et al.*, 2009, 2012; *Steiner et al.*, 2013]. Single profile observational RMS errors are estimated to be 0.7–1 K between 8 and 25 km, while for climatologies the observational, sampling, and systematic errors add to be within 0.15 K in this altitude range for the low to middle latitudes [*Steiner et al.*, 2011]. Initialization and ionospheric residual effects are the main contributors to systematic errors above ~25 km [*Steiner et al.*, 2011]. The current underutilization of RO data for stratospheric studies is exemplified by work of *Wee and Kuo* [2014].

3. Data

3.1. COSMIC Data

The U.S./Taiwanese COSMIC (also known as Taiwan's Formosa Satellite Mission #3) network is a mission consisting of six radio receivers on low-Earth-orbiting satellites in circular 72° inclination orbits that has been ongoing since April 2006 [*Anthes et al.*, 2008]. The COSMIC network produces around 1000–2000 profiles per day; however, lost communication with various satellites (including the FM3 satellite since August 2010) has caused the number of profiles to decrease over time. Data are obtained from the UCAR COSMIC Data Analysis and Archive Center (CDAAC) at http://cdaac-www.cosmic.ucar.edu/cdaac/products.html. The postprocessed "cosmic" dry temperature product (version 2010.2640) is used and referred to here as "COSMIC." ERA-40 Interim reanalysis model data that are collocated with the COSMIC mission profiles are also used from the CDAAC. Applied quality control consists of excluding profiles flagged "bad."

3.2. AIRS Data

NASA's AIRS and AMSU sensors are located on the Earth Observing System Aqua satellite and have been collecting data since September 2002. Data is obtained from the Goddard Earth Sciences Data and Information Services Center (http://disc.sci.gsfc.nasa.gov). The Level 2 (L2) version 6.0 Support Product (AIRX2SUP.006) temperature granules and Level 3 (L3) version 6.0, daily 1° × 1° gridded temperature products (AIRX3SPD.006) are used and are defined on the AIRS 101 pressure levels. Quality control of the L2 retrievals consists of using the quality flag labeled "Pbest," which determines how deep into the atmosphere the retrieval is considered to be valid [*Susskind et al.*, 2011; *Strow et al.*, 2003b]. The Level 3 product has a different signal-to-noise regime than the Level 2 product since it is an average of clearer sky scenes. For radiances, the Level 1 (L1) version 5 AIRIBRAD files are used.

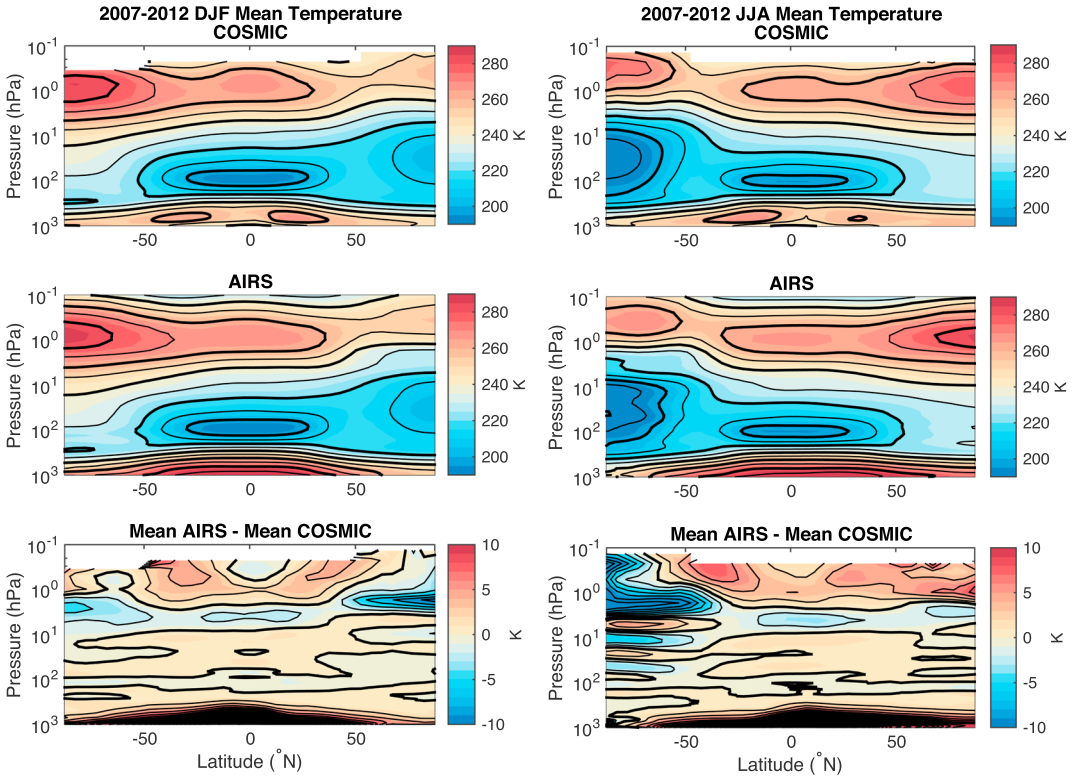

Figure 1. Five degree zonal mean temperatures over 2007–2012 for (left column) DJF and (right column) JJA seasons for COSMIC (top row, contoured bold every 20 K and thin every 10 K), AIRS L3 (middle row, contoured bold every 20 K and thin every 10 K), and AIRS L3 mean minus COSMIC mean temperature (bottom row, contoured bold at 0 K and thin every 2 K).

3.3. Case Study Data

Radiosonde data were obtained from the Atmospheric Radiation Measurement (ARM) Program sponsored by the U.S. Department of Energy, Office of Science, Office of Biological and Environmental Research, Climate and Environmental Sciences Division, through the ARM data archive (http://www.archive.arm.gov/armlogin/login.jsp). Vaisala-processed profiling data from balloon-borne sounding systems was used (twpsondewnpn).

4. Complete Temperature Data Set Comparison

4.1. Methods

In this section, AIRS daily L3 1° gridded products are used. Ascending and descending orbit products are averaged together to provide an estimate of the zonal daily mean. COSMIC dry temperature profiles, available on an altitude scale, are interpolated to the AIRS 101 pressure levels using the coincident pressure profile provided within the COSMIC dry temperature file. The COSMIC profiles are not gridded prior to zonal averaging due to their uniform distribution through time and longitude. The 6 year time period 2007 through 2012 is used to compute mean estimates of temperature by pressure, latitude zone, and season.

4.2. Results

For the monthly, 5° zonal scales shown, COSMIC provides roughly 2000 samples in the midlatitudes, 1000 in the tropics, and just under 500 poleward of ±80°N where the number of samples from AIRS also decreases. Figure 1 shows COSMIC and AIRS L3 mean temperatures for the December, January, and February (DJF) season and the June, July, and August (JJA) season over 2007–2012. The stratosphere's polar winter vortices, summertime warm mesosphere, and cold tropical tropopause are all evident features in these analyses. However, differences between the mean COSMIC and mean AIRS temperatures in Figure 1 (third row) show that greater than 10 K magnitude differences exist around 1 hPa. The

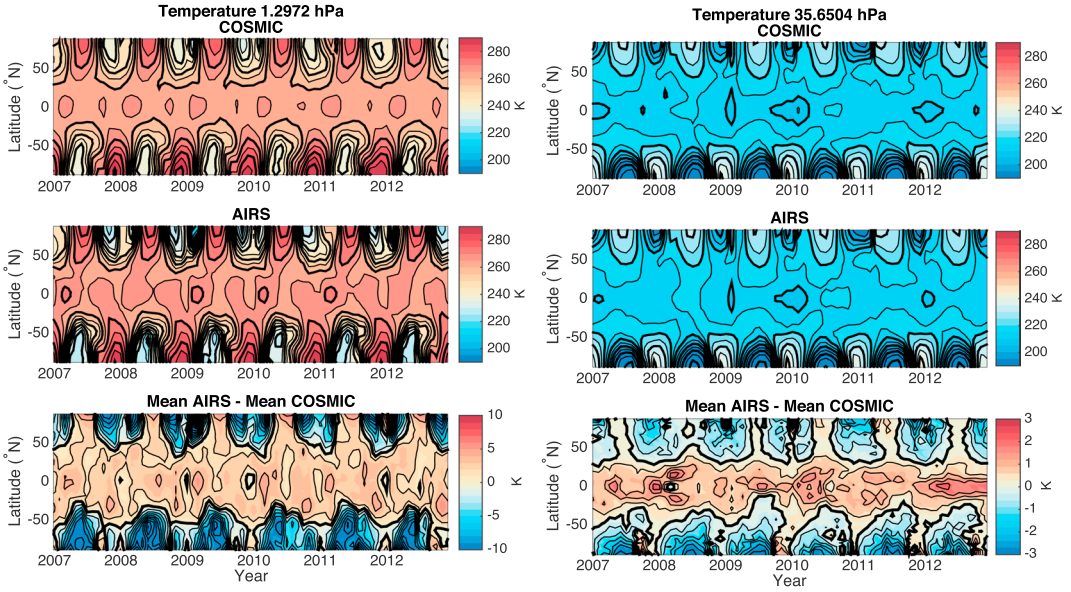

Figure 2. (top row) Monthly, 5° zonal COSMIC mean temperature (contoured bold (thin) every 10 K (5 K)) and (middle row) AIRS mean temperature (contoured bold (thin) every 10 K (5 K)) for the (left column) ~1 hPa and (right column) ~35 hPa pressure levels. (bottom row) Difference of the mean COSMIC and mean AIRS temperatures for same pressure levels (where left is contoured bold at 0 K and thin every 2 K, and right is contoured by bold at 0 K and thin every 0.5 K).

positive, lower tropospheric differences are due to the RO dry temperature assumption of zero water vapor. A "vertical layering" of the differences (positive and negative oscillation with height) in the JJA climatology's Southern Hemisphere (SH) polar region extends from 50°S to 90°S and is due to vertical oscillations in the AIRS profiles [*Feltz et al*., 2014b].

Figure 2 shows AIRS and COSMIC mean temperatures and their differences for two pressure levels—one in the lower middle (~35 hPa, or ~25 km) and one in the higher middle (~1 hPa, or ~45–50 km) stratosphere. The monthly, zonal temperature variation, seen previously in MSU and SSU data [e.g., *Young et al*., 2011; *Yulaeva et al*., 1994], is a result of the Brewer Dobson circulation, which is also known as the stratospheric meridional residual circulation and is characterized by air rising in the tropics and descending in polar regions. Signatures of sudden stratospheric warming events over the North Pole at 1 hPa (e.g., winter 2009–2011) are seen more clearly by the AIRS instrument at these scales, likely due to the RO's heavier reliance on climatology at these altitudes. Again, Figure 2 (third row) shows mean AIRS minus mean COSMIC differences. At 1 hPa in the high-latitude spring to summer time AIRS is colder than COSMIC by up to 20 K, while in the tropics AIRS is warmer than COSMIC by over 4 K. At 35 hPa AIRS and COSMIC generally agree within 2 K except in Antarctic winter time periods, where AIRS is again colder than COSMIC. Multiple hypotheses could explain the large differences in the winter polar zones seen at both pressure levels. Possible contributors include sparse polar sampling coverage by AIRS or COSMIC, a negative refractivity screening in the COSMIC temperature processing that could produce a warm temperature bias [*Foelsche*, 2014], the AIRS version 6 "vertical oscillation" that was identified in the Antarctic winter months [*Feltz et al*., 2014a], and ionospheric/initialization errors in the RO product.

Figure 3 shows global and tropical histograms overlaid with normal distributions for the 1 and 35 hPa level monthly, zonal differences shown in Figure 2. The global, 1 hPa level differences are skewed toward negative differences and are clearly non-Gaussian. At 35 hPa, the global histogram is more Gaussian shaped, which suggests that random processes could dominate error sources, but the spatiotemporal temperature patterns seen in Figure 2 suggest that multiple, nonrandom processes are contributing. The tropical histograms are somewhat more normally distributed, skewed slightly at 35 hPa to positive differences; nonetheless, a chi-square goodness of fit test shows none of the distributions are significantly normal. The mean, standard deviation, and uncertainty of the mean for the monthly, zonally averaged differences are shown in the figure titles. Here as well as in later analyses, the uncertainty of the mean is calculated as the standard deviation divided by the square root of the number of samples. The uncertainty of the mean is lower in the tropics

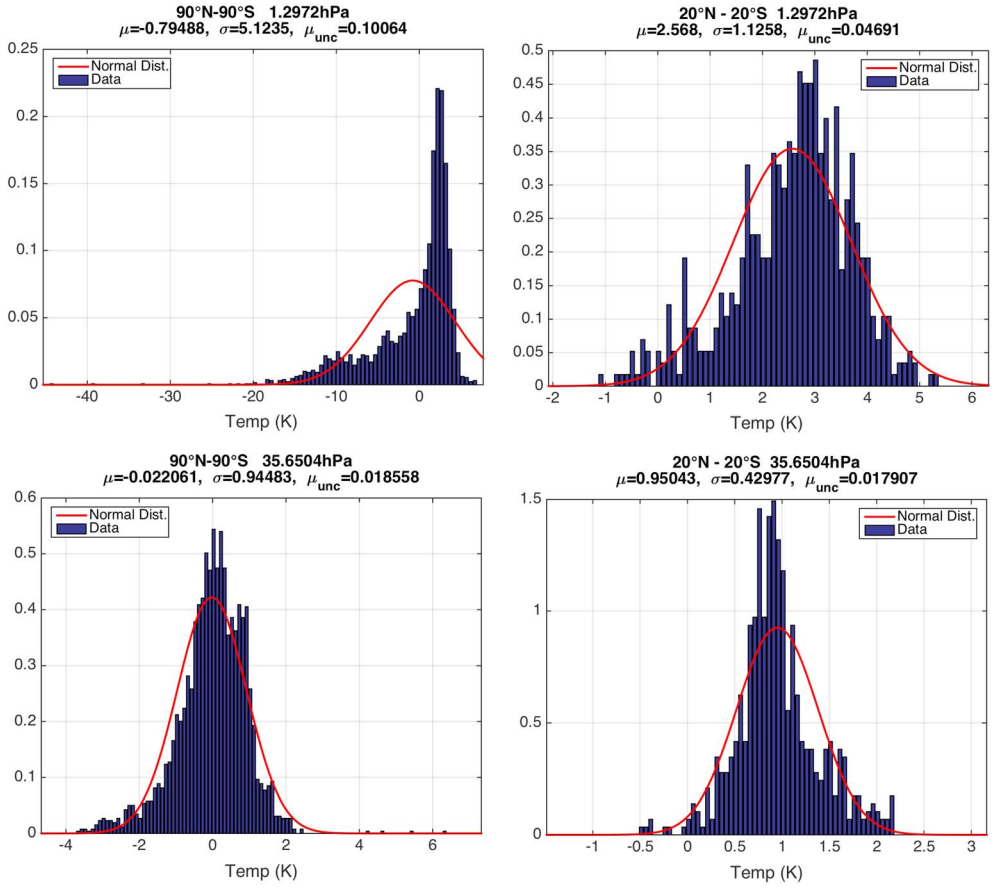

Figure 3. Histogram and normal distribution of the monthly, 5° zonal mean AIRS minus mean COSMIC temperatures at (top) ~1 h Pa and (bottom) ~35 hPa for the (left column) global and (right column) ±20 tropical region. The mean μ, standard deviation, and uncertainty of the mean are listed in title. See Figure 2 (bottom row) for corresponding maps of the differences. The normal distribution is created from the mean and standard deviation calculated from the histograms population.

at 35 hPa, which demonstrates how different regions and different altitudes have varying uncertainties in data sets and offer different opportunities for trending studies.

This analysis illustrates that zonal mean AIRS and zonal mean COSMIC temperatures exhibit systematic vertical and latitudinal difference patterns that vary with season. While qualitatively similar patterns are seen across latitude and time in the data sets, the magnitude of the differences warns that either one or both of AIRS and COSMIC products have characteristics that need to be understood more fully before using the data sets in climate studies. These differences between mean values could be ascribed to (1) sampling differences of the RO and IR sounder in time and space, (2) measurement errors, or (3) temperature retrieval errors. Section 5 addresses possibility (1) and later section 6 addresses possibilities (2) and (3).

5. Matchup Temperature Data Set Comparison

5.1. Methods

The RO and IR sounder matchup analysis uses the AIRS L2 granule-based profile products. The profile-to-profile matchup method finds COSMIC and AIRS L2 profiles that are coincident in time and space by using a 1 h time restriction between profiles and calculating a "raypath-averaged" IR sounder profile that is matched in space to the COSMIC RO profile. This raypath-averaged IR profile captures the unique variation of the RO profile's latitude and longitude with height, as well as the theoretical horizontal resolution along the occultation ray path [*Feltz et al.*, 2014a]. Matchup numbers vary with season and latitude but globally are ~300 per day or ~7000–11,000 per month with matchups being densest in polar regions. Quality

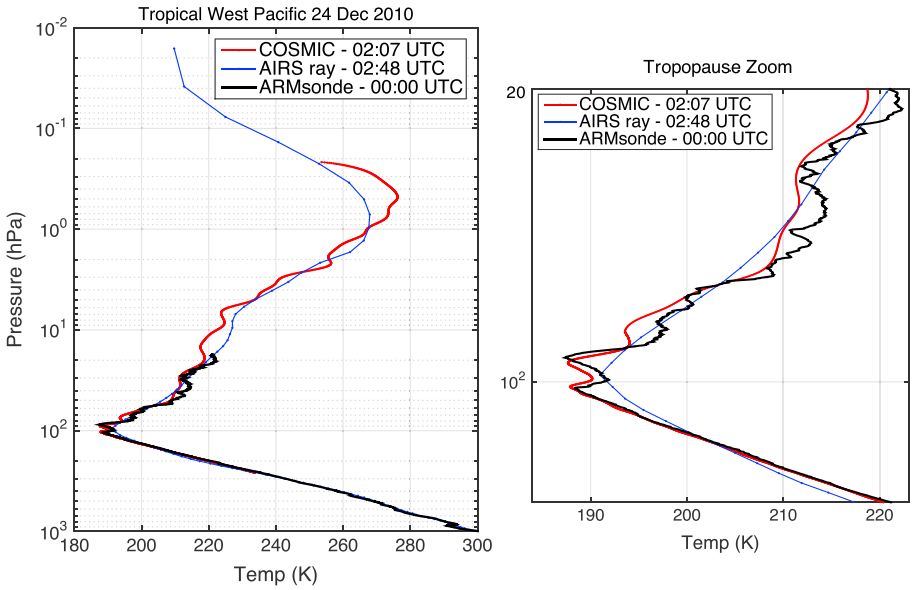

Figure 4. The 24 December 2010 Tropical West Pacific Nauru Island ARM radiosonde, COSMIC, and AIRS (left) raypath-averaged matchup temperatures shown with a (right) zoomed view of the tropopause region. Matchup times noted in the legend.

control includes excluding matchup cases where the AIRS or COSMIC temperature profile has missing values between 1 and 100 hPa.

Vertical temperature averaging kernels (AKs) are also introduced in this section to account for the different vertical resolving capabilities of the RO and hyperspectral IR sounding instruments. The AKs used in this study are distinguished from the AIRS operationally produced retrieval AKs and represent what vertical resolution the stratospheric peaking hyperspectral IR channels are theoretically capable of, not what is output by the AIRS Version 6 L2 retrieval algorithm. Being dependent on the atmospheric state, the AIRS AKs used in this study are calculated using ERA-Interim temperature profiles and a radiative transfer model. The AKs are applied to the AIRS minus COSMIC difference for every matchup case. This method is designed to provide a generalized approach to project temperature profiles onto a uniform vertical grid, more details are given in Appendix A1 and *Feltz et al*. [2017]. Temperature differences which have the AK applied represent how well the RO and IR sounder retrievals agree at the IR sounders measurement resolution, i.e., vertical structure that is at a resolution higher than the AIRS sensor resolving capability is removed by application of the theoretical AK. In the following text, temperature differences which have the AIRS AKs applied are referred to as "AK smoothed temperatures" or are denoted by "AK*" in figures.

5.2. Results

This section addresses the spatiotemporal mismatch errors of section 4's AIRS L3 and COSMIC comparison by applying a profile-to-profile matchup method to AIRS L2 and COSMIC profile data. An example matchup case between an AIRS L2, COSMIC, and ARM radiosonde profile from the ARM Tropical West Pacific site is shown in Figure 4 with temperatures overlaid (no AKs applied). Measurement times are noted in the legend, and although the sonde's release time was over 2 h earlier around 00 UTC, it did not reach 100 hPa until approximately an hour later, closer to the time of the AIRS and RO measurements. The COSMIC profile contains more vertical structures than AIRS, and over 5 K differences are seen in the stratosphere. The zoomed view of the tropical tropopause in Figure 4 (right) illustrates how COSMIC is able to pick up the fine, oscillatory feature, most likely caused by the presence of inertial gravity waves, that the AIRS profile smooths over. Subsequent results show that the effects of mismatch errors are relatively small for our applications.

Next, AIRS temperature averaging kernels are applied to the AIRS L2 minus COSMIC differences. To investigate the effect of the temperature profile used to calculate the AK on the AK smoothed differences, AKs are calculated for both the AIRS retrieved temperature and the coincident ERA temperature state

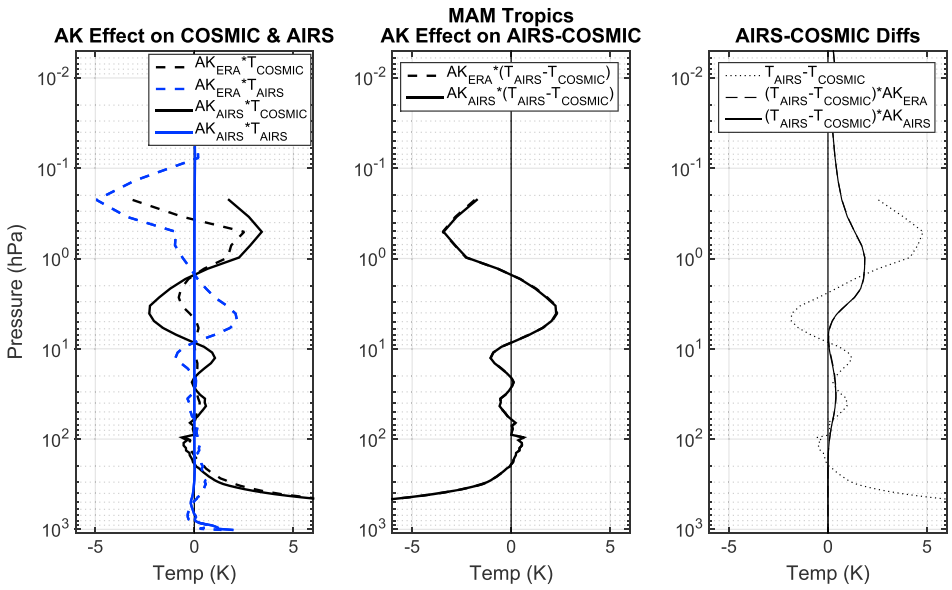

Figure 5. (left) Different effects of the AK_{AIRS} and AK_{ERA} application to AIRS and COSMIC temperatures, calculated as $T_{COSMIC} - T_{COSMIC}$ *AK and $T_{AIRS} - T_{AIRS}$ *AK, respectively. (middle) Effect of the AK_{AIRS} and AK_{ERA} application to the AIRS-COSMIC differences are shown, calculated as $(T_{AIRS} - T_{COSMIC})$-$(T_{AIRS} - T_{COSMIC})$*AK and also (right) shows $T_{AIRS} - T_{COSMIC}$ difference biases with different vertical smoothings applied.

(referenced as AK_{AIRS} and AK_{ERA} respectively, with all other atmospheric variables being similar) and applied to the AIRS minus COSMIC differences. Figure 5 illustrates the effects of the two different AK's application on the COSMIC and AIRS temperatures, as well as the AIRS-COSMIC differences for the tropical March/April/May season. Figure 5 (left) shows that the AK_{ERA} affects both the AIRS and COSMIC temperatures, while the AK_{AIRS} affects only the COSMIC profile. Nonetheless, both AKs have very similar effects on the AIRS-COSMIC difference as seen in Figure 5 (middle and right). Differences between the effects of the AK applications are confined to altitudes above ~10 hPa and are largest in the polar zones (not shown). Due to the similarity of the AK_{AIRS} and AK_{ERA} effects on the temperature differences and for simplicity purposes in the forward calculations required for the AK computations, all following results make use of AK_{AIRS}.

Results of the matchup method and AK application are shown for monthly, zonal scales in Figure 6 as the average of the AIRS minus COSMIC matchup differences with (bottom row) and without (top row) AKs applied for two pressure levels (the same levels as shown in Figure 2). These resulting difference biases are based on a subset of the complete data set (seen in Figures 2 and 3). When no AK is applied, the matchup

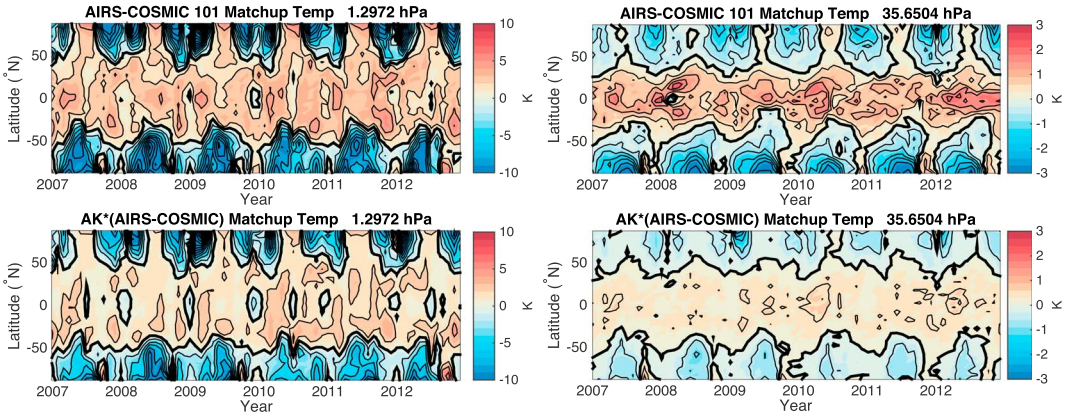

Figure 6. Monthly, 5° zonal bias of the AIRS-COSMIC matchup data set differences for the (left column) 1 hPa and (right column) 35 hPa levels without (top row) and with (bottom row) AIRS AKs applied (see Figure 2 (bottom row) for comparison to complete data set analysis).

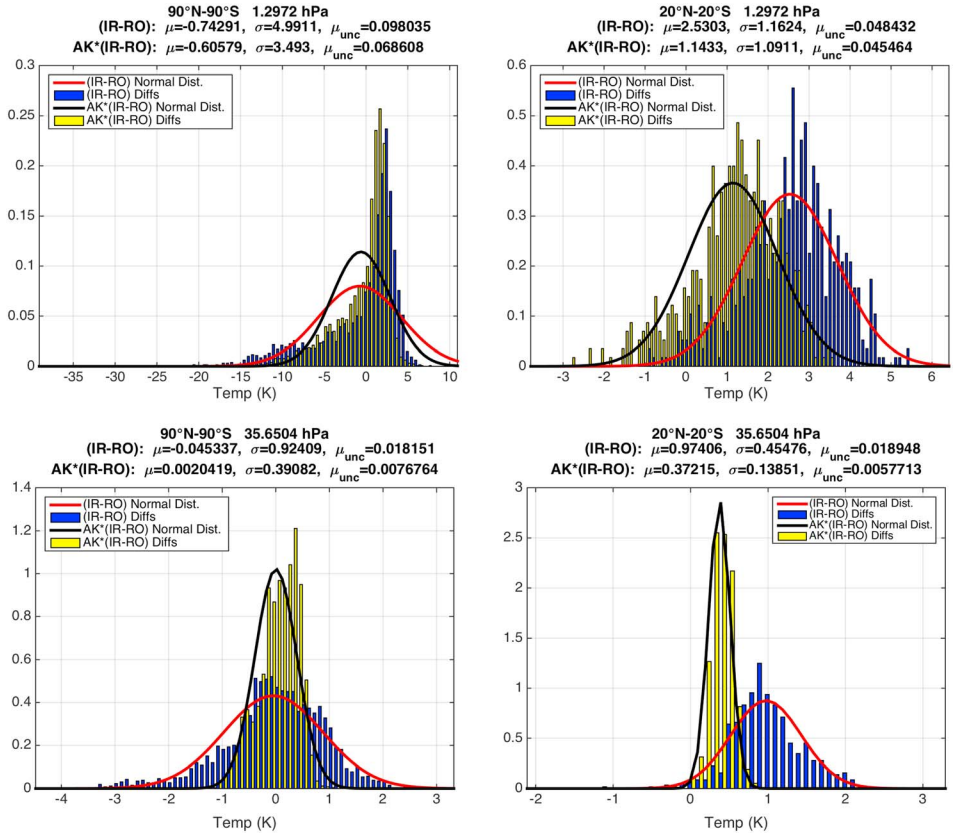

Figure 7. Histogram and normal distribution of the monthly, 5° zonal AIRS-COSMIC difference biases with (yellow) and without (blue) AK application at (top row) 1 hPa and (bottom row) 35 hPa for the (left column) global and (right column) ±20° tropical region. The mean μ, standard deviation, and uncertainty of the mean are listed in title. See Figure 6 (bottom row) for corresponding maps.

and complete data sets show similarity with only small differences visible, for example, where the matchup data set bias is decreased around 2009 at 90°N (see Figure 2 and Figure 6, top row). In general, AK application decreases the matchup data set difference biases, but a similar pattern of the temperature bias is seen across latitude and time. Figure 7 shows the corresponding global and tropical histograms of the monthly, 5° zonal matchup data set difference biases with and without AK application. Comparison of these histograms with those from the complete data set in Figure 3 reinforces the similarity between the complete data set and the matchup data set where no AK is applied—the distributions for these data sets in Figures 3 and 7 appear largely unchanged. When the AK is applied, the histograms show a reduced standard deviation and bias.

Table 1 compares statistical measures of the AIRS L2 minus COSMIC differences before and after application of the matchup method and AKs for global and five latitude zones. Specifically, the mean, standard deviation,

Table 1. Statistical Measures of the 35 hPa Level Monthly, 5° Zonally Averaged AIRS Minus COSMIC Temperature Differences for the Complete Data Sets and Matchup Subsets[a]

	Complete Data Set			Matchup Data Set, No AK Application			Matchup Data Set, AK Application		
Latitude	Mean	SD	Mean Uncertainty	Mean	SD	Mean Uncertainty	Mean	SD	Mean Uncertainy
90N–90S	−0.02206	0.9448	0.01856	−0.04534	0.9241	0.01815	0.04950	0.5961	0.01171
90N–60N	−0.4799	0.9424	0.04534	−0.6045	0.6677	0.03213	−0.3639	0.3853	0.01854
60N–30N	−0.1912	0.4065	0.01956	−0.1629	0.3895	0.01874	0.005386	0.2186	0.01052
30N−30S	0.8042	0.4478	0.01524	0.8198	0.4777	0.01625	0.3495	0.1453	0.004943
30S−60S	−0.1238	0.3981	0.01915	−0.1209	0.4089	0.01967	−0.03009	0.2956	0.01972
60S−90S	−0.9458	1.1315	0.05444	−1.0233	1.0583	0.05092	−0.2981	0.3532	0.01699

[a]Units given in kelvin. The mean uncertainty is calculated as the standard deviation (SD) divided by the square root of the number of samples.

and uncertainty of the mean are found using the 5° zonally averaged AIRS minus COSMIC differences over the latitude bounds shown in Table 1. Estimates of mean differences for the complete and matchup data sets that have no AK applied are in agreement within the estimated uncertainty for each zone except for the northern polar zone. This similarity reveals that spatiotemporal sampling errors are not dominant contributors to the mean AIRS-mean COSMIC differences at these time and space scales. However, AK application significantly changes the mean differences in all zones. While the global bias change is small with the AK application, individual latitude zones see a decrease in the bias.

6. Matchup Brightness Temperature Comparison

6.1. Methods

In this section, AIRS measured radiances are introduced as a reference standard for the matchup data set. For every AIRS and COSMIC matchup case, a merging of coincident AIRS radiance channels is performed, so that the AIRS L1B 3 × 3 radiance measurement footprint (which corresponds to a single L2 retrieval field of view) that is closest to the RO profile's latitude/longitude at each assigned pressure level is extracted. When selecting the matching radiance, the 3 × 3 "golf ball" mean for the specific AIRS channel whose weighting function height matches the RO height is selected. Using this method, radiances for different channels are represented by measurements taken at coincident latitudes and longitudes based on the RO profile geometry.

AIRS radiances and temperature Jacobians are calculated for each matchup case for both the COSMIC and AIRS L2 temperature profiles using the Optimal Spectral Sampling (OSS) fast radiative transfer model (RTM), which has an accuracy of 0.05 K brightness temperature with respect to a reference line-by-line model [*Moncet et al*., 2008, 2015]. Focus is confined to the 15 μm region, carbon dioxide absorption bands. Parameters describing the atmospheric state, aside from air temperature, are identical for both the AIRS and COSMIC calculations. Because the AIRS and COSMIC profiles do not extend the entire vertical range of the radiative transfer model (RTM), missing data values in the COSMIC and AIRS input temperatures are filled using a climatology and introduce methodological uncertainties in the calculations. Since AIRS profiles typically have values reported up to the RTM top, the COMIC profiles are merged into the AIRS profiles before missing data values are filled, so that the radiance differences are most representative of the actual temperature difference. Uncertainties due to missing data exist in general for channels whose weighting functions (WFs) peak at altitudes higher than the ~10 hPa (~30 km) level. Largest sensitivities to missing data treatment are seen in the ~667.53–668.45 cm^{-1} channels whose WFs peak in the upper stratosphere, while channels such as the 666.7740 cm^{-1} are sensitive by an amount which is negligible for this study. Appendix A3 documents the calculated radiance sensitivity to (1) discontinuities in the input temperature profiles and (2) carbon dioxide input profiles, while further details of the RTM calculation methodology are given in Appendix A2.

6.2. Results

To aid in interpretation of section 5's AK smoothed COSMIC minus AIRS L2 matchup differences, the simulated radiances from the AIRS and COSMIC profiles are compared to AIRS measured radiances. To leverage the AIRS measurements as an absolute reference, a threshold radiometric uncertainty of 0.5 K brightness temperature (BT) is used to discuss the results. This threshold is motivated by the fact that AIRS radiances are very stable over orbit, the time of day, and from day to day. Thus, this study defines good agreement to the AIRS measurements as being within 0.5 K BT. When a measurement minus calculation bias is greater than 0.5 K, it is concluded that there is an error in the retrieved temperature used to perform the calculation. Figures in this section show radiance results in units of BT.

Figure 8 shows overlaid, robust-lowess filtered daily averaged time series of BT and temperature differences which represent the lower middle stratosphere for a global and 5 latitude zones. Temperatures are shown for ~35 hPa (~25 km) and are overlaid with the 666.7 cm^{-1} channel BTs, whose weighting function (WF) maximum is also at ~35 hPa. Figure A1 in Appendix A1 illustrates this channel's WF and depicts the vertical slab layer for which the channel is sensitive. For all zones, the COSMIC calculated minus AIRS measured BT bias shows qualitatively similar seasonal structure to the AK smoothed COSMIC minus AIRS temperatures, with the corollary being that the AIRS calculated minus AIRS measured BT biases generally lack seasonal

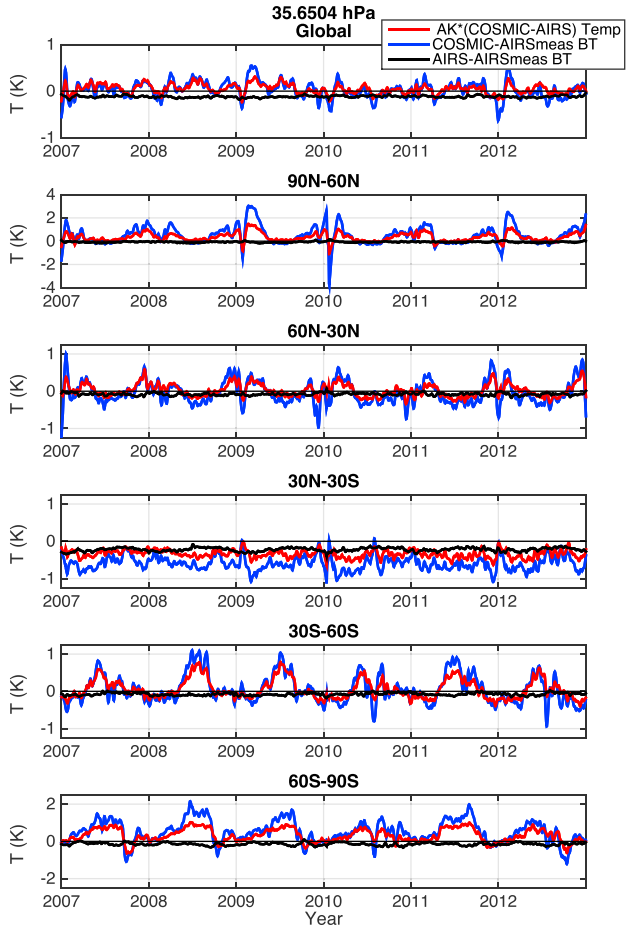

Figure 8. Global and zonal time series of robust Lowess filtered daily averages for six latitude zones at the ~35 hPa level for AK*(COSMIC-AIRS) temperature (red), COSMIC calculated minus AIRS measured 666.7 cm^{-1} BTs (blue), and AIRS calculated minus AIRS measured 666.7 cm^{-1} BTs (black). (Note *y* scale changes for polar zones.)

structure and are close to zero. For all zones, the AIRS calculated BTs agree to the measured BTs within the 0.5 K uncertainty. Where COSMIC BT differences are greater than 0.5 K, there is confidence that the corresponding COSMIC temperature retrievals contain errors. While both the BT and temperature biases at ~35 hPa remain under 0.5 K in the global average, biases reach up to 1 K and 2 K in the midlatitudes and polar zones, respectively. Differences are largest in polar winters, with COSMIC calculated BTs being warmer than the measured BTs by over 1 K.

Figures 9 and 10 show zonal BT differences as a function of height as well as the COSMIC minus AIRS temperatures with and without the AK applied for the JJA and DJF seasons, respectively, for latitude zones that are consistent with those of Figure 8. BT differences are plotted at the heights of the channel's WF peaks and are overlaid with horizontal and vertical error bars representing their mean uncertainty and channels' WFs full widths at half max, respectively. Except for the Tropics, BT and temperature difference biases are seen to be variant across the DJF and JJA season, implying the presence of seasonally varying bias sources. AIRS BT biases are generally within the 0.5 K uncertainty range for altitudes below 3 hPa, with an exception for the JJA Antarctic. AIRS calculated BTs transition from being slightly cooler than the measured BTs at altitudes below ~3 hPa to being warmer above. COSMIC BTs also become increasingly warmer than the measured BTs with height, most drastically in the polar zones. For channels whose WFs peak around 30 hPa (where confidence in the BT calculations is highest) COSMIC biases are generally less than the 0.5 K AIRS radiometric uncertainty. Exceptions to this standard imply errors in the COSMIC temperatures and exist in the JJA Antarctic and both DJF polar zones where the COSMIC BT biases are positive, and in the tropics where BT biases are cool and lie just outside of the 0.5 K uncertainty range. COSMIC minus AIRS temperature differences mirrors this structure. Lastly, the AIRS and COSMIC calculated BT difference, which is representative of the true AIRS and COSMIC product difference for all channels, is seen to be over 2 K for certain zones, notably the JJA Antarctic and both DJF polar zones.

Lastly, Figure 11 shows monthly, 5° zonally averaged 666.7 cm^{-1} BT and ~35 hPa level temperature biases. Biases on these spatiotemporal scales are larger, but the AIRS calculated BTs overall still agree with the AIRS measurements within the 0.5 K uncertainty. COSMIC's BT bias is often above 1 K and sometimes 3 K in the polar wintertime. The bias also holds similar qualitative spatiotemporal structure to the smoothed temperature difference, where a warm, polar, early winter month bias occurs in tandem with a cold, tropical region bias. Patterns of the biases motivate the idea that zonal latitudinal analyses should be used in satellite temperature product validation. Global averages over larger time scales can mask characteristics of biases that aid in the determination of their sources.

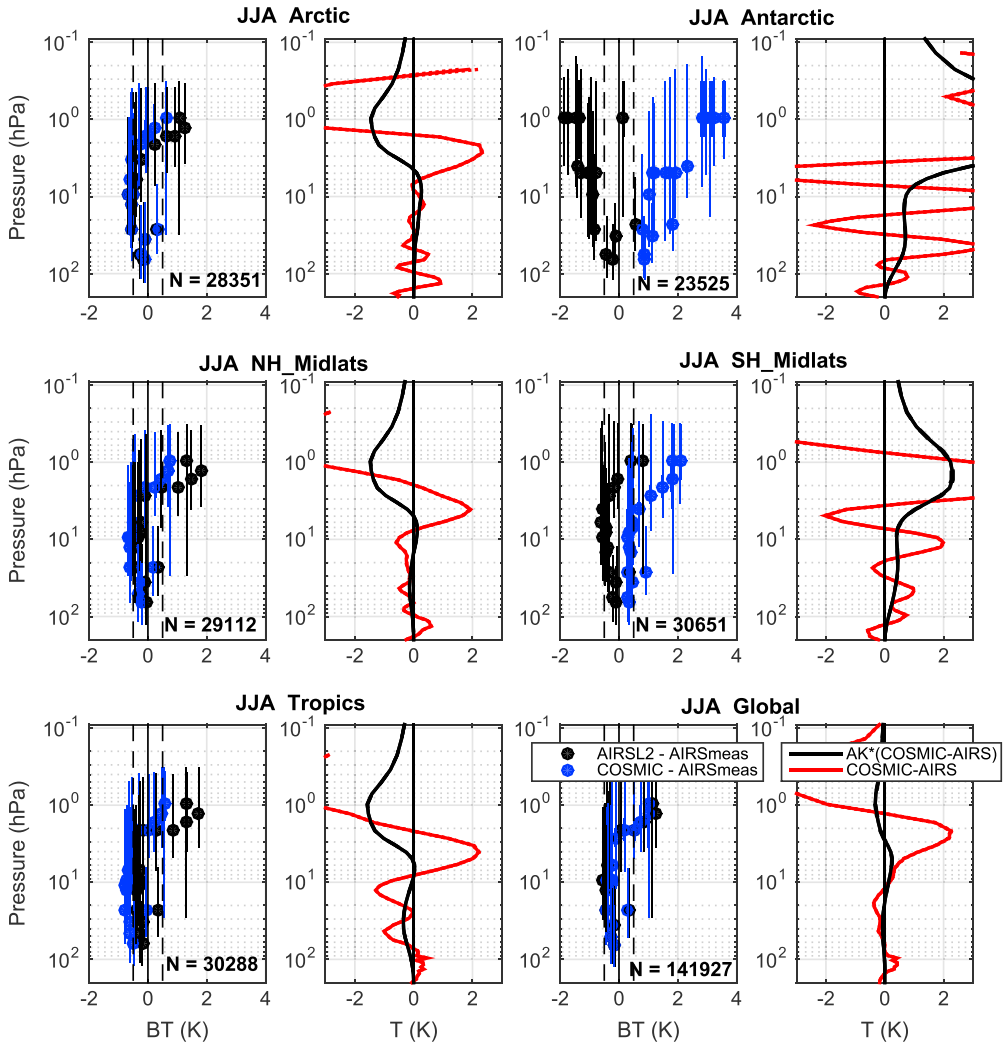

Figure 9. Zonal and global analyses for June, July, and August. AIRS (black) and COSMIC (blue) calculated minus AIRS measured BT biases plotted at the height of the channels WF maxima (dots) with horizontal and veritcal bars denoting uncertainty of the bias and the full width at half max of the WF, respectively (black dashed lines mark the <0.5 K AIRS measurment uncertainty) (right panels). COSMIC minus AIRS temperature bias and uncertainty with (black) and without (red) the AK applied (left panel). Number of samples, *N*, noted in the figure.

7. Discussion

In section 4, differences between the complete data sets of AIRS L3 and COSMIC temperatures revealed characteristic patterns in space and time on monthly, 5° zonal scales, with magnitudes that reached over 10 K in the stratosphere. Uncertainty of the mean differences were computed for different latitude zones at 35 hPa, which were found to be smallest for the tropics, and demonstrated how data sets at different regions and altitudes have varying uncertainties and offer different opportunities for trending studies. Application of the profile-to-profile matchup method and the AIRS vertical averaging kernels to the AIRS L2 and COSMIC products in section 5 indicated that the majority of the AIRS and COSMIC differences within the stratosphere are not the product of the differences in instrument sampling in time and space or vertical resolution, but rather, they are a product of differences in retrieval errors. AK application had the largest effect in polar regions and reduced the matchup differences on monthly and seasonally averaged, zonal scales by over 3 K in the upper stratosphere and 1 K in the lower stratosphere. In general, the application of AKs improved COSMIC and AIRS agreement, but it did not remove the seasonal difference biases, indicating that there are seasonally dependent systematic errors which have a vertical resolution that the AIRS instrument is not able to resolve.

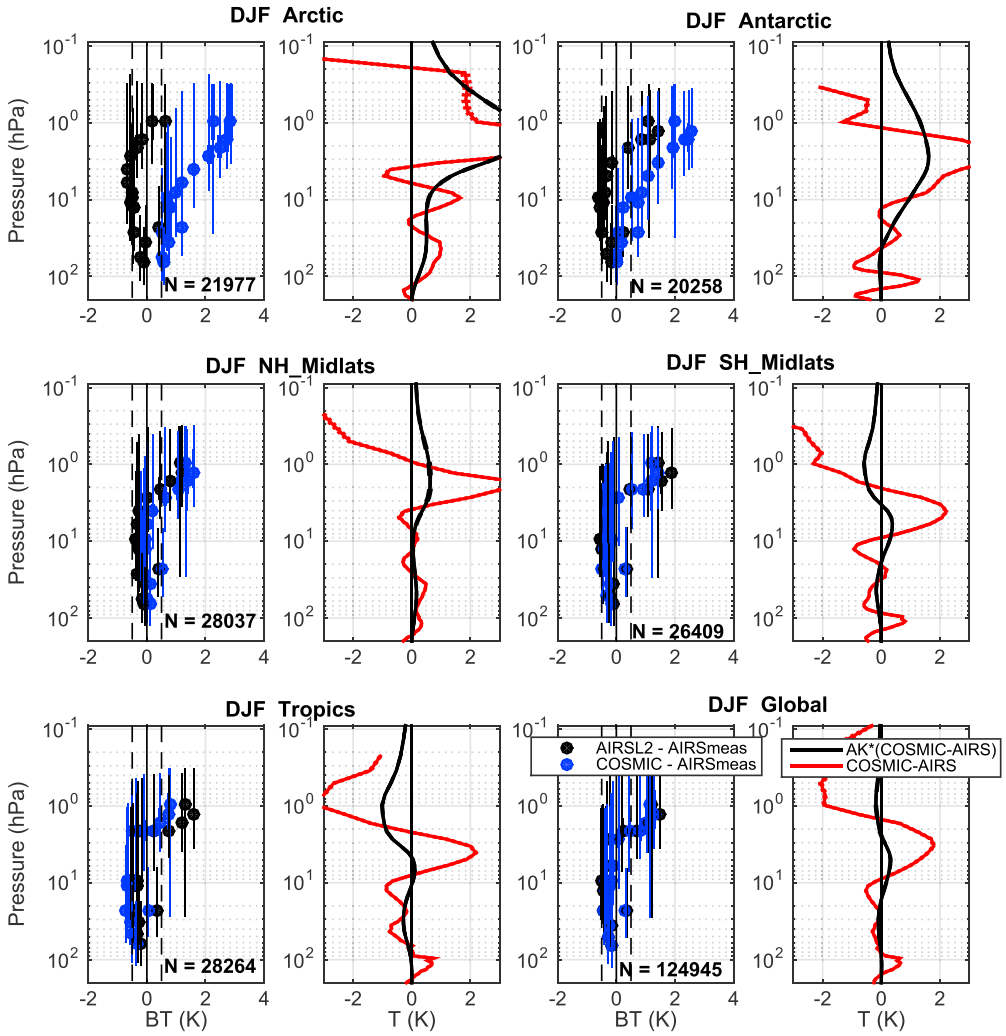

Figure 10. Same as Figure 9 but for December, January, and February.

In section 5, the COSMIC and AIRS AK smoothed temperature differences revealed a warm bias in the AIRS L2 product in the Tropics around ~35 hPa (~25 km)—Table 1 shows that between 30N and 30S an ~0.8 K warm bias exists when no AKs are applied, and an ~0.3 K warm bias remains when AKs are applied. This AIRS tropical warm bias is also reflected in the time series result of Figure 8 and monthly, zonal differences of Figure 11 where the AK*(COSMIC-AIRS) difference is negative. For more information on this bias, the reader is referred to *Feltz et al*. [2017].

In section 6, Figures 9 and 10 showed that the difference between the calculated BTs, or the equivalence of the AIRS calculated minus COSMIC calculated BTs, is often the same sign and a similar magnitude as the corresponding AIRS minus COSMIC temperatures. The general disagreement between the AIRS measured and calculated BTs seen at altitudes above ~3 hPa (~40 km) in Figures 9 and 10 could be attributed to either methodological errors or the fact that the calculated AKs do not account for the AMSU microwave information which is used by the AIRS operational algorithm. This is due to the fact that one could expect an AIRS temperature retrieved using only IR information to agree with the radiances from which it was derived. Such a "consistency check" on this agreement of the AIRS calculated and measured radiances could not be expected to reveal null space errors (i.e., errors that results from the lack of a unique solution to the retrieval problem [*Rodgers*, 1990]) in the AIRS temperature profile. For example, the JJA Antarctic AIRS calculated BTs were not far from agreement with the measured BTs, but analyses indicated the presence of large, unphysical vertical oscillations in the L2 AIRS temperature product.

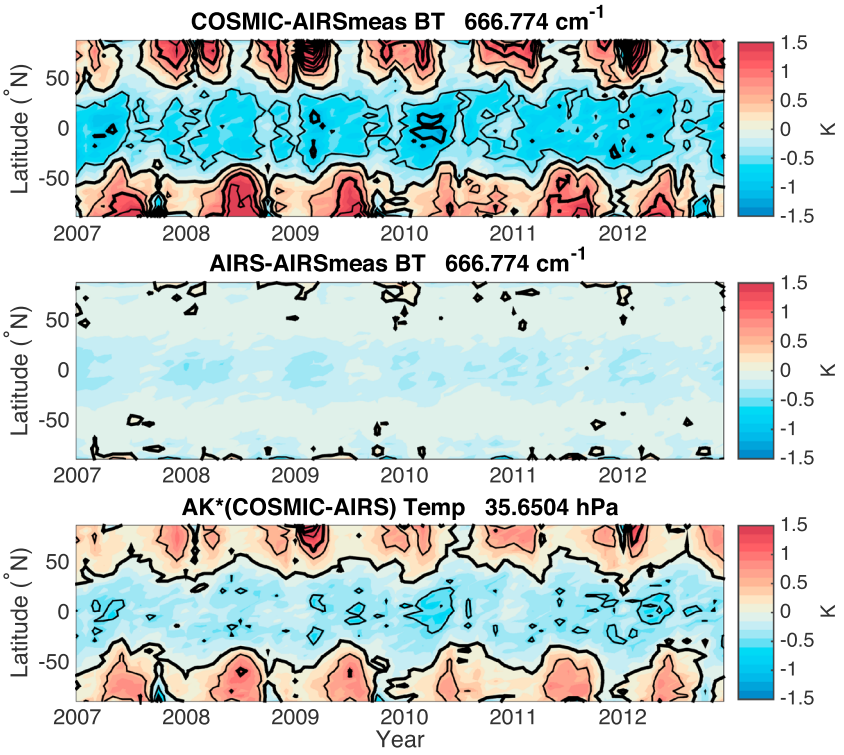

Figure 11. Monthly, 5° zonal (top) COSMIC and (middle) AIRS calculated minus measured AIRS BTs for the 666.7 cm^{-1} channel and (bottom) AK*(COSMIC-AIRS) temperature at ~35 hPa.

A significant COSMIC minus AIRS measured BT bias was found for channels with WF peaks between ~100 and 10 hPa in (1) the JJA Antarctic zone where most channels showed COSMIC BTs to be more than 0.5 K warmer than AIRS measurements and (2) the DJF polar zones where select channels show a COSMIC BT bias of greater than 0.5 K. On smaller scales, in the filtered, daily time series and monthly, 5° zonal analyses, COSMIC is seen to have greater than 0.5 K differences most commonly in polar winter regions, as is consistent with the seasonal results, and they have good agreement at other times such as in midlatitude summers. From these results, a COSMIC polar region, warm bias that grows with height in the stratosphere is implied and is consistent with the fact that RO is most accurate in the UTLS but has higher altitude errors due to ionospheric uncertainties.

8. Conclusions

This study demonstrated an assessment of radio occultation and hyperspectral infrared sounder temperature profile products using infrared radiances. For the COSMIC RO network and AIRS sounder, the sampling of spatiotemporally coincident measurements was sufficient to estimate zonal means for 0130 and 1330 local times. Application of AIRS temperature averaging kernels reduced the magnitudes of the differences between COSMIC and AIRS temperature profiles so that the differences were found to be consistent with the calculated minus measured BT differences. The COSMIC calculated minus AIRS measured BTs exceeded a 0.5 K threshold for extratropical latitude zones in the winter hemisphere. These differences are attributed to seasonal UCAR COSMIC retrieval biases, possibly due to ionosphere first guess dependence. Unphysical vertical oscillations are seen in the AIRS L2 temperature product in austral winter Antarctic regions, and results imply a small AIRS tropical warm bias around ~35 hPa (~25 km) in the middle stratosphere.

A study done by *Das and Pan* [2014] that compares COSMIC and Sounding of the Atmosphere using Broadband Emission Radiometry (SABER) temperatures from December 2010 to November 2011 provides stimulating comparisons (see *Das and Pan* [2014] Figure 2). Like the COSMIC BT differences, *Das and Pan* [2014]

finds that COSMIC dry temperatures for all seasons and zones also transition from being cooler than their reference, SABER, to being warmer at ~1–5 hPa. Specifically, COSMIC is shown to be ~2 K cooler below ~1–5 hPa (~38–50 km) and over 5 K warmer above at ~0.3 hPa (~60 km). However, while *Das and Pan* [2014] concludes, "COSMIC data can be used with confidence up to 1 hPa," results shown here caution the use of COSMIC data for certain seasons and latitude zones at pressures greater than 1 hPa (altitudes less than ~50 km)—though it is recognized that the necessary degree of accuracy varies with the analysis being performed.

Another recent study that yields an interesting comparison opportunity is that of *Ladstädter et al.* [2015] which compares multiple radiosonde data sets to RO data from three different missions [see *Ladstädter et al.*, 2015, Figure 4]. *Ladstädter et al.* [2015] finds that over the coincident time period of this study, 2007–2012, global, annual RO differences from radiosondes in both the 30–100 hPa and 30–10 hPa layer are mostly positive, having a rough upper bound at 0.3 K, with the higher altitude stratospheric layer having larger magnitude differences. Global, monthly time series of COSMIC and AIRS differences show qualitatively similar results.

While the results motivate the need for future work on making AIRS and COSMIC temperature products more accurate for certain latitude zones and time periods, specifically polar regions, it also demonstrates the potential use for RO and IR sounders in monitoring stratospheric temperatures. The basic accuracy of the hyperspectral infrared sounder radiances and radio occultation bending angles are proving to be adequate for application to the study of stratospheric change. However, additional work needs to be done to better understand the systematic errors of the methods used to derive stratospheric temperature profiles. Future work will involve expanding the comparison of hyperspectral IR sounders and GPS RO products to include additional sensors and alternate processing methods including the CrIS and IASI sounders and GRAS sensors.

Appendix A: Auxiliary Details

A1. Temperature Averaging Kernels

AIRS temperature averaging kernels (AKs) are calculated using simulated AIRS temperature Jacobians. The Jacobians, also referred to as weighting functions, describe the portions of the profiles represented by each radiance measurement [*Rodgers*, 1976]. A Tikhonov regularization approach using a damping parameter computed by singular value decomposition is used to condition the inverse matrix in the AK calculation. The AK represents the smoothing that a retrieval from the specific set of radiances induces, and the width of each AK curve is a measure of the vertical resolution of the observing system [*Rodgers*, 1976]. As in *Rodgers* [1990], the averaging kernel, $\hat{A}$, is related to atmospheric temperature, and the retrieved temperature, x_{ret}, by

$$(x_{\mathrm{ret}} - x_{\mathrm{o}}) = \hat{A}(x - x_{\mathrm{o}}). \tag{A1}$$

A smoothed version, x_{smooth}, of a higher resolution profile such as the RO profile in this study, x, may then be calculated by [*Connor et al.*, 1994; *Rodgers and Connor*, 2003]

$$x_{\mathrm{smooth}} = x_{\mathrm{o}} + \hat{A}(x - x_{\mathrm{o}}), \tag{A2}$$

and the smoothed IR sounder minus RO temperature difference by

$$(x_{\mathrm{ret}} - x)_{\mathrm{smooth}} = (x_{\mathrm{ret}} - x_{\mathrm{o}}) - \hat{A}(x - x_{\mathrm{o}}). \tag{A3}$$

In the above equations, x_{o} is set to be the temperature profile used to compute the Jacobian [*Rodgers*, 1990; *Rodgers and Connor*, 2003], and for this study is defined using the AIRS temperature profile. Figure A1 shows an example AIRS weighting function (WF) and its associated AK for an AIRS, global temperature profile averaged over 2007–2012. Channels whose WFs have the least contribution from altitudes above ~1 hPa, where no COSMIC data is available, have the smallest methodological uncertainties associated with them. These channels, such as the 666.774 cm^{-1} channel, have WFs that peak at altitudes below ~30 hPa. Further details of the AK calculation process can be found in the appendix of *Feltz et al.* [2017].

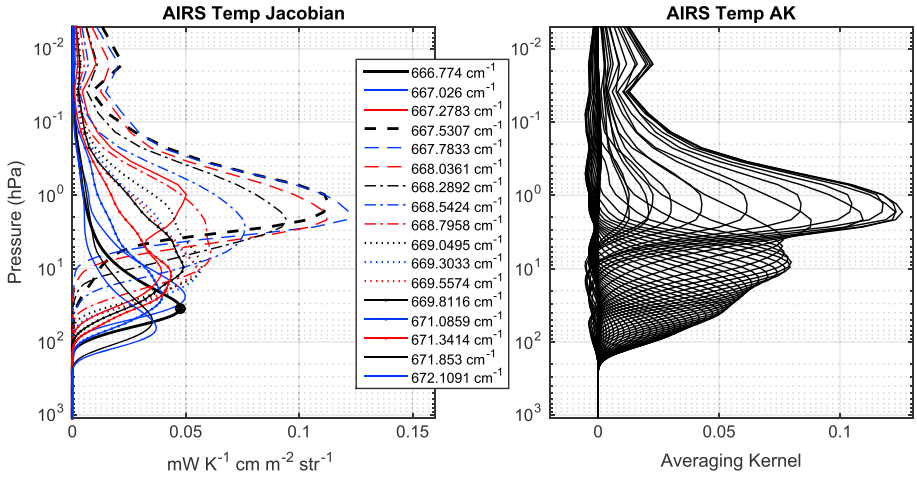

Figure A1. AIRS global, (left) averaged temperature Jacobian for the years 2007 through 2012 and (right) associated averaging kernel. Dot indicate channels whose weighting function maxima occur at ~35 hPa.

A2. Radiative Transfer Calculations

A2.1 Model Input Data

Carbon dioxide (CO_2) data are obtained from CarbonTracker (CT), NOAA's Earth System Research Laboratory CO_2 measurement and modeling system. Version CT2013, available for 2000–2012 as global 3° × 2° gridded monthly CO_2 mole fractions, is used [*Peters et al*., 2007; http://carbontracker.noaa.gov].

Ozone, skin temperature, and surface pressure are obtained from ECMWF's ERA-Interim reanalysis model [*Dee et al*., 2011; *Berrisford et al*., 2011; http://www.ecmwf.int/en/research/climate-reanalysis/era-interim]. The ERA output provides global grids at six hourly increments. The 0.75° gridded, model level product is used, which reports output up to vertical pressure levels of ~0.1 hPa. This corresponds to a horizontal resolution of ~80 km.

A2.2 Method

Forward calculations of AIRS radiances and temperature Jacobians are performed using the Optimal Spectral Sampling (OSS) radiative transfer model (RTM) [*Moncet et al*., 2008]. The legend of Figure A1 lists the set of channels for which radiances and Jacobians are calculated. Atmospheric state and RTM parameters, aside from air temperature, are kept consistent between the COSMIC and AIRS calculations but are varied for every matchup case. The model does calculations on 101 pressure levels which are consistent with the levels that the AIRS 101 level products are reported on, and the top of the model is defined as 1.0E−3 hPa. A default solar zenith angle of 89° is used, and radiances are simulated for the view angle corresponding to the mean scan angle of the AIRS L1B 3 × 3 radiance golf ball for which the AIRS matchup temperature profile is retrieved.

CarbonTracker monthly, 2° zonal averages are used to define CO_2 profiles. The CO_2 average closest in space to the matchup latitude and which corresponds to the month and year in which the matchup took place is used. The CarbonTracker profiles typically cover from 0.5 hPa to the surface level (1100 hPa), and the profiles are extended to be to be constant with height above and below the levels with available data.

ECMWF's ERA-Interim reanalysis is used to define surface pressure, skin temperature, ozone, and water vapor. Water vapor profiles that are interpolated to the time and location of the COSMIC profiles are obtained through UCAR's CDAAC. Surface pressure, skin temperature, and ozone profiles are obtained directly from ECMWF, and the ERA-Interim time step and grid point that is closest in time and space to the matchup is used. Because the ERA-Interim products are only reported up to ~1 hPa and do not cover the entire vertical range of the model domain, Air Force Geophysics Laboratory (AFGL) Atmospheric Constituent Profiles [*Anderson et al*., 1986] of ozone are used to "fill the gaps" at altitudes above and below the ERA-Interim profiles. The day of year and latitude determines which AFGL model atmosphere is used, i.e., subarctic winter/summer, midlatitude winter/summer, or tropical.

Assignment of the RTM input temperature profiles requires more careful attention. For consistency in how the COSMIC and AIRS profiles are treated, COSMIC profiles (which don't extend to as high of altitudes as

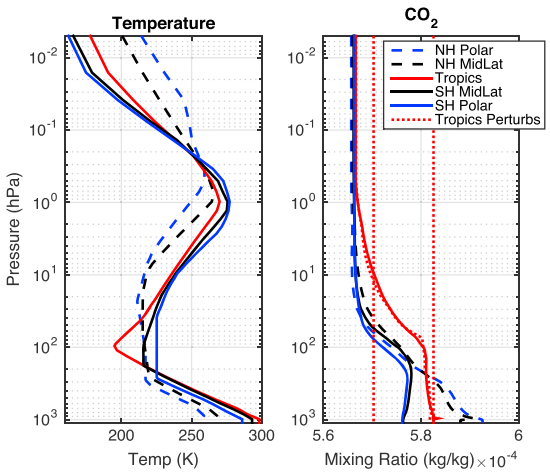

Figure A2. Carbon dioxide sensitivity study input. (left) AFGL temperatures and (right) control run CO_2 profiles (solid lines) for the five atmosphere cases with the tropical atmosphere perturbation run CO_2 profiles (dotted red lines) overlaid.

AIRS) are first merged into the AIRS profiles and lastly are inserted into the AFGL profiles. Using this method to fill missing data values, the COSMIC and AIRS calculated radiance difference is the most representative of the temperature difference. There can be "discontinuities," or large, above 10 K jumps in the COSMIC or AIRS input temperature profile between levels where information comes from different sources (i.e., from AFGL, COSMIC, or AIRS). This "discontinuity phenomenon" is most common in the COSMIC NH midlatitude winter input profiles, and it adds a methodological uncertainty to the calculated radiances. Thus, care is taken in the interpretation of simulated radiance results for channels whose WFs have significant contributions from regions where there is no COSMIC data (above ~1 hPa).

A3. Calculated Radiance Sensitivity Studies

A3.1 Carbon Dioxide

Sensitivity of the radiances to carbon dioxide is investigated for five atmospheres which represent different latitude bands during January 2007. For each zonal atmosphere, radiances are calculated for four different CO_2 profiles. These four profiles include a control profile, which is defined by a 2° zonal, monthly average, and three perturbation profiles which are defined by the following: a 3-hourly, 3 × 2° profile estimate, and two constant with height profiles whose magnitudes are determined by the surface and 10 hPa control profile CO_2 value. The control and perturbation CO_2 profiles are shown for the tropical atmosphere case in Figure A2 (right), and the other zonal atmosphere's control profiles are overlaid. The temperature profiles for each zonal atmosphere, defined by the AFGL model atmospheres, are shown in Figure A2 (left).

Figure A3 shows the results of the CO_2 perturbations in BT units. Seen in Figure A3 (middle), the constant with height surface value profile produced the largest BT differences from the control run for all atmospheres with the maximum difference reaching ~0.25 K in the SH polar zone. The constant with height 10 hPa value profile shows a maximum change of just over 0.025 K occurring for the tropical case. Using a constant with height CO_2 profile defined by a single mean value can be an attractive simplification in the radiance calculation, but as seen by these results, the use of a single surface value could lead to errors in a single BT calculation of over 0.25 K and possibly introduce a small warm bias for these channels. The BT differences for the 3-hourly, 3 × 2° CarbonTracker CO_2 profile are not shown since magnitudes are negligible for this application (under 0.01 K). This supports the viable simplification of using of monthly, zonally averaged CO_2 profiles rather than 3-hourly 3 × 2° profiles for input to the radiance calculations.

A3.2 Temperature

Sensitivity of the radiances to temperature is investigated for two different phenomena. The first phenomenon is an example temperature profile discontinuity which results from the process of filling in data gaps at the surface and top of atmosphere (TOA) profile levels where no temperature data are available from the RO or IR sounder retrievals (see details in Appendix A2). The altitudes of these temperature discontinuities in the COSMIC input profiles vary on a case by case basis, but typically, they lie between the 0.34 hPa and 0.13 hPa pressure levels. AIRS retrievals usually have values reported up to the TOA, so discontinuities are rarer. Perturbations from the control temperature profile for this study include discontinuities that are inserted at the 0.34 hPa and 0.13 hPa pressure levels. The magnitudes of the perturbations are determined by an example, monthly average discontinuity magnitude—that from January 2007 which is 12 K.

The second phenomenon investigated is a hypothetical RO temperature profile structural bias. The example used is a bias profile taken from *Feltz et al.* [2014b], which was found between UCAR's previous versions of

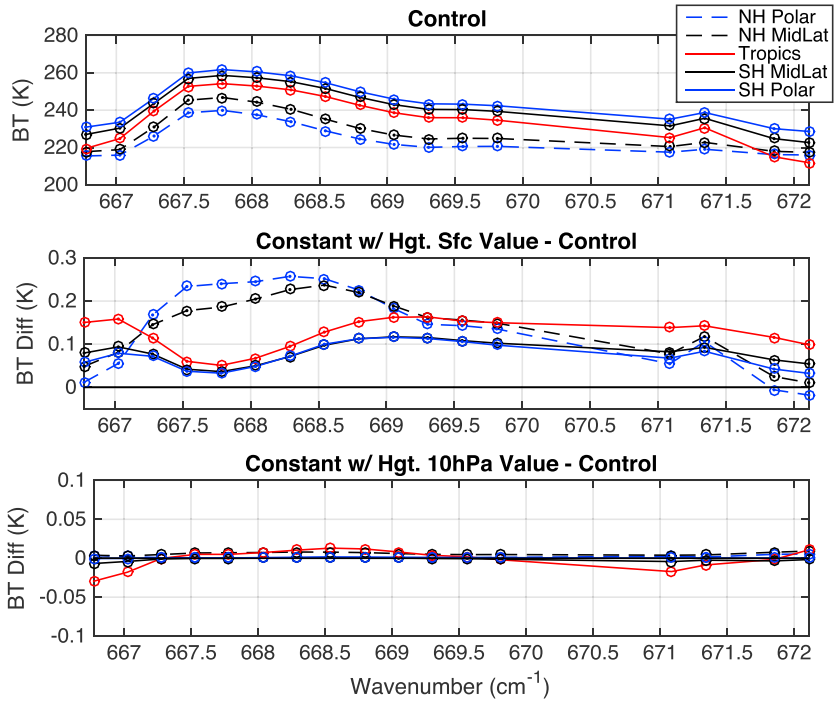

Figure A3. Carbon dioxide sensitivity study results. BT calculations for the (top) five zonal atmosphere control runs, and (middle) BT differences of the constant surface value minus control run and (bottom) constant 10 hPa value minus control run.

COSMIC and Global Navigation Satellite System Receiver for Atmospheric Sounding (GRAS) temperature data sets. Specifically, the bias was for the January 2007 NH midlatitude GRAS minus COSMIC differences and was detected by a double difference using IASI temperatures. A perturbation is done to see whether this bias, when converted to BT units, is large enough such that the AIRS measurements could be used to diagnose if COSMIC or GRAS were more accurate.

The control profile, defined by the AFGL winter midlatitude atmosphere, and its variations are shown in Figure A4 (left), while Figure A4 (middle) shows the perturbation minus control differences. The corresponding

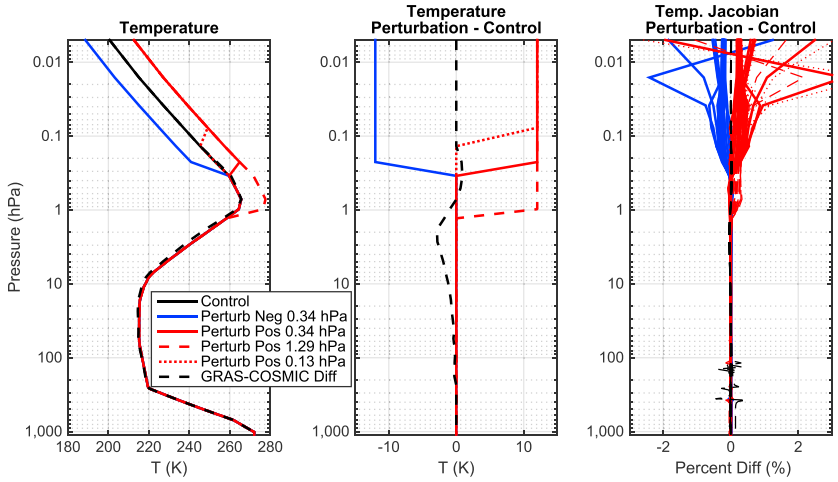

Figure A4. Temperature sensitivity study. (left) Control and perturbation temperatures, (middle) perturbations minus control temperature differences, and (right) percent differences of the calculated perturbation minus control temperature Jacobians. Temperature Jacobian differences are plotted for 17 channels which are listed in Figure A1.

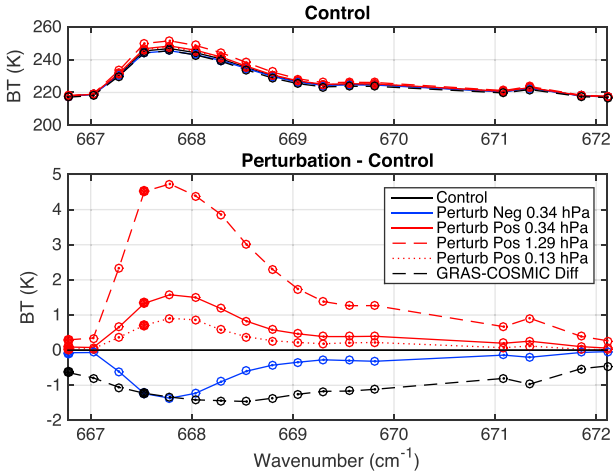

Figure A5. Temperature sensitivity study. (top) Control and perturbation computed BTs and (bottom) perturbation minus control BT differences with filled circles indicating locations of channels of focus.

sensitivities of the temperature Jacobians are shown as percent differences in Figure A4 (right). The Jacobians are sensitive to the inserted temperature profile discontinuities above the altitudes at which the discontinuities are introduced, while the example RO structural bias produced the most evident changes between 400 and 100 hPa of less than 1% in the Jacobians. Corresponding simulated BTs and control minus perturbation BT differences are shown in Figure A5. As the height of the temperature discontinuity decreases, the change in BT for all channels increases. Table A1 shows the change in BT per 1 K change in the magnitude of the 0.34 hPa level temperature discontinuity. While the significance of a BT uncertainty varies with the analysis context, the 666.7 cm^{-1}, 0.34 hPa temperature discontinuity 0.0074 BT (K)/temperature (K) effect is primarily negligible in this study since the estimated AIRS measurement uncertainty is 0.5 K; thus, a 67 K discontinuity in temperature at 0.34 hPa is necessary for the computed BT discontinuity effect to be equivalent to the AIRS measured BT uncertainty. In contrast, the 667.5 cm^{-1} channel is much more sensitive to the discontinuity effect, experiencing a 0.1111 K/K change, which would require a mere 4.5 K magnitude discontinuity for the discontinuity effect to be larger than the 0.5 K BT threshold.

The BT change produced by the GRAS minus COSMIC bias is more consistent across channels and is confined below 1.5 K. For certain channels (and thus corresponding atmospheric levels which the channels represent), the change is large enough so that a theoretical comparison of forward calculated GRAS and COSMIC BTs to the AIRS measured BTs could enable a statistically significant difference. From such an analysis, it could be determined whether COSMIC or GRAS temperatures are more consistent with the AIRS measured BTs; however, this topic is outside the scope of this paper.

A3.3 Hypothetical RO Temperature Uncertainty Profile

Sensitivity of the radiances to a hypothetical RO dry temperature uncertainty profile is calculated for five zonal atmospheres. The RO uncertainty profiles for each latitude zone are estimated by the standard deviation of the ERA 40 reanalysis minus COSMIC temperature differences over the corresponding latitude zone for January 2007. Figure A6 shows these uncertainty profiles, as well as the resulting perturbation minus control BTs. The uncertainty profiles for all zones have maxima between 5 and 15 K near the surface due to water vapor contamination of the dry temperature products. The NH middle latitude and polar zone uncertainties have additional maxima at ~1–2 hPa which heavily influence the BT results. While the tropics and SH zones' BT changes are confined between 1–3 K, the NH BT changes reach up to 5 and 6 K for AIRS highest peaking stratospheric channels.

Table A1. Calculated BT Sensitivity to Temperature Discontinuity Effect at 0.34 hPa[a]

cm^{-1}	**666.77**	667.03	667.28	**667.53**	667.78	668.04	668.29	668.54	668.80	669.05	669.30	669.56	669.81	671.09	671.34	671.85	672.11
BT (K)/T (K)	**0.007**	0.006	0.055	**0.111**	0.131	0.125	0.099	0.069	0.048	0.039	0.032	0.032	0.033	0.017	0.021	0.008	0.005

[a]Uncertainty determined by a 0.34 hPa, 12 K temperature discontinuity perturbation run. Bold entries are for channels which are focused on in later analyses.

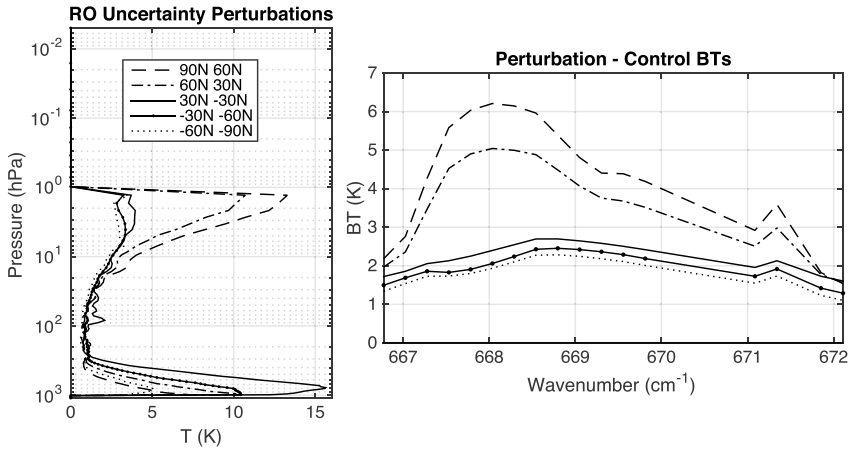

Figure A6. BT Sensitivity study to RO temperature uncertainty. (left) Ersatz RO temperature uncertainties defined by the standard deviations of ERA 40 minus COSMIC temperature differences for five latitude zones in January 2007 with (right) corresponding overlaid RO temperature uncertainty perturbed minus control BT differences for all five zones.

The NH polar zone BT difference is further investigated by perturbing the NH polar uncertainty profile over three different vertical regions of the atmosphere. Figure A7 shows three different perturbations of the NH polar uncertainty profile that are performed between the TOA, 10 hPa, 300 hPa, and surface. Resulting BT differences also seen in Figure A7 show that the considered AIRS channels are insensitive to temperature below 300 hPa and that channels between 667.5 cm^{-1} and 668.5 cm^{-1} are dominantly sensitive to the temperature at altitudes above 10 hPa. Channels at the very edge of the spectra shown around

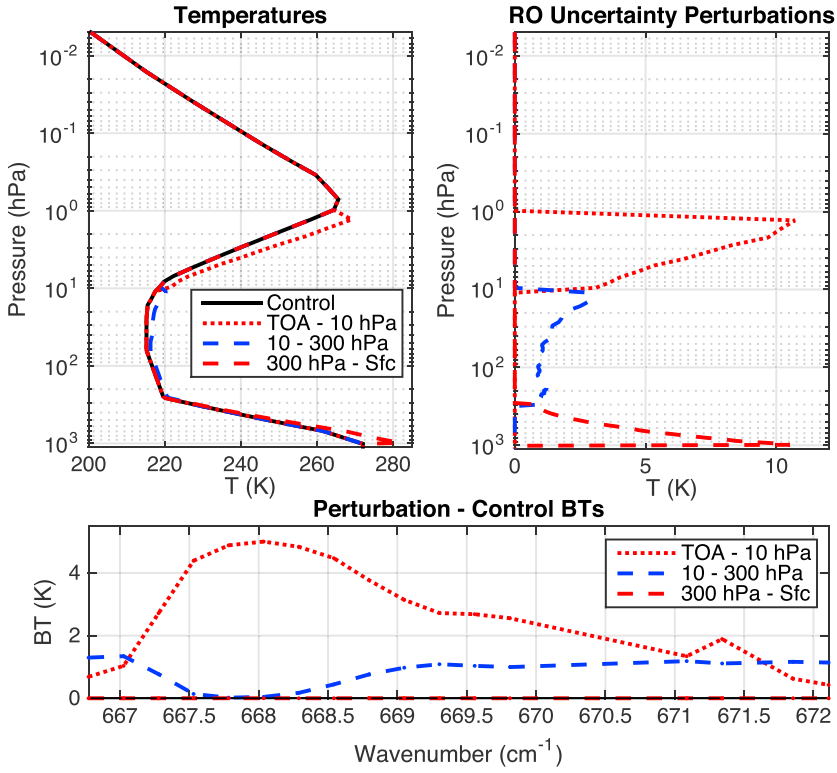

Figure A7. Temperature uncertainty sensitivity study. (top right) Control and perturbation RO uncertainty temperature profiles, (top left) perturbation minus control differences, and (bottom) corresponding BT differences for the January 2007 NH polar zone.

~667 cm^{-1} and 672 cm^{-1} are more sensitive to temperature within the 10–300 hPa region than to altitudes above 10 hPa. Knowing what atmospheric levels that the AIRS channels are more or less sensitive to aids in interpretation of the simulated and measured AIRS BT differences. These perturbations reveal that the AIRS measured radiances, assuming an estimated 0.5 K uncertainty, would be able to diagnose a temperature profile error that is the magnitude of an estimated RO uncertainty profile.

Acknowledgments

Thanks are given to Matthew Hitchmann, Tristan Le'cyer, and Steven Ackerman of the University of Wisconsin-Madison Atmospheric and Oceanic Sciences Department for reviewing this work when it was first presented as part of a Master's thesis. Likewise, acknowledgments are given to the reviewers of this paper, who added a lot of insight and gave many helpful comments. This work was funded under NOAA grant NA10NES4400013 and NASA grant NNX15AC26G. NASA AIRS products were obtained from the Goddard Earth Sciences Data and Information Services Center (GES DISC) funded by NASA's Science Mission Directorate. Acknowledgment is given to the NPSO (Taiwan's National Space Organization) and UCAR (University Corporation for Atmospheric Research) for access to the COSMIC data. ARM data were obtained from the Atmospheric Radiation Measurement (ARM) Climate Research Facility, a U.S. Department of Energy Office of Science user facility sponsored by the Office of Biological and Environmental Research. The data used in this study were supported by the Office of Biological and Environmental Research of the U.S. Department of Energy as part of the Atmospheric Radiation Measurement (ARM) Climate Research Facility, an Office of Science user facility. Data sources are referenced in section 3.

References

Alexander, P., A. Torre, P. Llamedo, and R. Hierro (2014), Precision estimation in temperature and refractivity profiles retrieved by GPS radio occultations, *J. Geophys. Res. Atmos.*, *119*, 8624–8638, doi:10.1002/2013JD021016.

Anderson, G. P., S. A. Clough, F. X. Kneizys, J. H. Chetwynd, and E. P. Shettle (1986), AFGL atmospheric constituent profiles (0.120 km), No. AFGL-TR-86-0110, Air Force Geophysics Lab Hanscom AFB, Mass.

Anderson, J. G., J. A. Dykema, R. M. Goody, H. Hu, and D. B. Kirk-Davidoff (2004), Absolute, spectrally-resolved, thermal radiance: A benchmark for climate monitoring from space, *J. Quant. Spectrosc. Radiat. Transfer*, *85*(3–4), 367–383.

Anthes, R. A., et al. (2008), The COSMIC/FORMOSAT-3 mission: Early results, *Bull. Am. Meteorol. Soc.*, *89*(3), 313–333.

Aumann, H. H., et al. (2003), AIRS/AMSU/HSB on the Aqua mission: Design, science objectives, data products, and processing systems, *IEEE Trans. Geosci. Remote Sens.*, *41*(2), 253–264.

Bani Shahabadi, M., Y. Huang, L. Garand, S. Heilliette, and P. Yang (2016), Validation of a weather forecast model a radiance level against satellite observations allowing quantification of temperature, humidity and cloud-related biases, *J. Adv. Model. Earth Syst.*, *8*, 1453–1467, doi:10.1002/2016MS000751.

Berrisford, P., et al. (2011), Atmospheric conservation properties in ERA-Interim, *Q. J. R. Meteorol. Soc.*, *137*(659), 1381–1399.

Board, S. S., National Research Council (2007), *Earth Science and Applications from Space: National Imperatives for the Next Decade and Beyond*, National Acad. Press.

Connor, B. J., D. E. Siskind, J. J. Tsou, A. Parrish, and E. E. Remsberg (1994), Ground-based microwave observations of ozone in the upper stratosphere and mesosphere, *J. Geophys. Res.*, *99*, 16,757–16,770, doi:10.1029/94JD01153.

Danzer, J., B. Scherllin-Pirscher, and U. Foelsche (2013), Systematic residual ionospheric errors in radio occultation data and a potential way to minimize them, *Atmos. Meas. Tech.*, *6*(8), 2169–2179, doi:10.5194/amt-6-2169-2013.

Das, U., and C. J. Pan (2014), Validation of FORMOSAT-3/COSMIC level 2 "atmPrf" global temperature data in the stratosphere, *Atmos. Meas. Tech.*, *7*(3), 731–742, doi:10.5194/amt-7-731-2014.

Dee, D. P., et al. (2011), The ERA-Interim reanalysis: Configuration and performance of the data assimilation system, *Q. J. R. Meteorol. Soc.*, *137*(656), 553–597.

Divakarla, M., C. Barnet, M. Goldberg, L. McMillin, E. Maddy, W. Wolf, L. Zhou, and X. Liu (2006), Validation of Atmospheric Infrared Sounder temperature and water vapor retrievals with matched radiosonde measurements and forecasts, *J. Geophys. Res.*, *111*, D09S15, doi:10.1029/2005JD006116.

Feltz, M. L., R. Knuteson, S. Ackerman, and H. Revercomb (2014a), Application of GPS radio occultation to the assessment of temperature profile retrievals from microwave and infrared sounders, *Atmos. Meas. Tech.*, *7*(11), 3751–3762, doi:10.5194/amt-7-3751-2014.

Feltz, M. L., R. O. Knuteson, H. E. Revercomb, and D. C. Tobin (2014b), A methodology for the validation of temperature profiles from hyperspectral infrared sounders using GPS radio occultation: Experience with AIRS and COSMIC, *J. Geophys. Res. Atmos.*, *119*, 1680–1691, doi:10.1002/2013JD020853.

Feltz, M. L., R. O. Knuteson, H. E. Revercomb, and D. C. Tobin (2017), Assessment of NOAA NUCAPS upper air temperature profiles using COSMIC GPS radio occultation and ARM radiosondes, *J. Geophys. Res. Atmos.*, *122*, doi:10.1002/2017JD026504.

Foelsche, U. (2014), On possible reasons for systematic errors in GPS radio occultation climatologies, their characterization, and potential ways to remove some of them, Eighth FORMOSAT-3/COSMIC Data Users' Workshop. UCAR Center Green Campus, Boulder, Colo. 2 October 2014. Conference Presentation.

Foelsche, U., et al. (2008), Observing upper troposphere–lower stratosphere climate with radio occultation data from the CHAMP satellite, *Clim. Dyn.*, *31*(1), 49–65.

Foelsche, U., et al. (2011a), Errors in GNSS radio occultation data: Relevance of the measurement geometry and obliquity of profiles, *Atmos. Meas. Tech.*, *4*(2), 189–199.

Foelsche, U., et al. (2011b), Refractivity and temperature climate records from multiple radio occultation satellites consistent within 0.05%, *Atmos. Meas. Tech.*, *4*(9), 2007–2018, doi:10.5194/amt-4-2007-2011.

Funatsu, B. M., C. Claud, P. Keckhut, A. Hauchecorne, and T. Leblanc (2016), Regional and seasonal stratospheric temperature trends in the last decade (2002–2014) from AMSU observations, *J. Geophys. Res. Atmos.*, *121*, 8172–8185, doi:10.1002/2015JD024305.

Gaffen, D. J. (1994), Temporal inhomogeneities in radiosonde temperature records, *J. Geophys. Res.*, *99*, 3667–3676, doi:10.1029/93JD03179.

Global Climate Observing System (GCOS) (2011), Systematic observation requirements for satellite-based data products for climate, WMO Tech. Doc. GCOS-154. 21.

Goody, R., and R. Haskins (1998), Calibration of radiances from space, *J. Clim.*, *11*(4), 754–758.

Goody, R. M., R. Haskins, W. Abdou, and L. Chen (1995), Detection of climate forcing using emission spectra, *Issled. Zemli iz Kosmosa*, *5*, 22–33.

Goldberg, M. D., H. Kilcoyne, H. Cikanek, and A. Mehta (2013), Joint polar satellite system: The United States next generation civilian polar-orbiting environmental satellite system, *J. Geophys. Res. Atmos.*, *118*, 13,463–13,475, doi:10.1002/2013JD020389.

Goldberg, M., et al. (2011), The global space-based inter-calibration system, *Bull. Am. Meteorol. Soc.*, *92*(4), 467.

Haimberger, L., C. Tavolato, and S. Sperka (2008), Toward elimination of the warm bias in historic radiosonde temperature records—Some new results from a comprehensive intercomparison of upper-air data, *J. Clim.*, *21*(18), 4587–4606.

Han, Y., et al. (2013), Suomi NPP CrIS measurements, sensor data record algorithm, calibration and validation activities, and record data quality, *J. Geophys. Res. Atmos.*, *118*, 12,734–12,748, doi:10.1002/2013JD020344.

Hartmann, D.L., et al. (2013), Observations: Atmosphere and surface, in *Climate Change 2013: The Physical Science Basis. Contribution of Working Group I to the Fifth Assessment Report of the Intergovernmental Panel on Climate Change*, edited by T. F. Stocker et al., pp. 159–254, Cambridge Univ. Press, Cambridge, U. K., and New York, doi:10.1017/CBO9781107415324.008.

He, W., et al. (2009), Assessment of radiosonde temperature measurements in the upper troposphere and lower stratosphere using COSMIC radio occultation data, *Geophys. Res. Lett.*, *36*, L17807, doi:10.1029/2009GL038712.

Hilton, F., et al. (2012), Hyperspectral Earth observation from IASI: Five years of accomplishments, *Bull. Am. Meteorol. Soc.*, *93*(3), 347.
Ho, S.-P., et al. (2009), Calibration of temperature in the lower stratosphere from microwave measurements using COSMIC radio occultation data: Preliminary results, *Terr. Atmos. Ocean. Sci.*, *20*, 87–100, doi:10.3319/TAO.2007.12.06.01(F3C).
Ho, S.-P., et al. (2012), Reproducibility of GPS radio occultation data for climate monitoring: Profile-to-profile inter-comparison of CHAMP climate records 2002 to 2008 from six data centers, *J. Geophys. Res.*, *117*, D18111, doi:10.1029/2012JD017665.
Hoffmann, L., and M. J. Alexander (2009), Retrieval of stratospheric temperatures from Atmospheric Infrared Sounder radiance measurements for gravity wave studies, *J. Geophys. Res.*, *114*, D07105, doi:10.1029/2008JD011241.
Huang, Y., V. Ramaswamy, X. Huang, Q. Fu, and C. Bardeen (2007), A strict test in climate modeling with spectrally resolved radiances: GCM simulation versus AIRS observations, *Geophys. Res. Lett.*, *34*, L24707, doi:10.1029/2007GL031409.
Huang, Y., S. Leroy, J. Gero, J. Dykema, and J. Anderson (2010), Separation of longwave climate feedbacks from spectral observations, *J. Geophys. Res.*, *115*, D07104, doi:10.1029/2009JD012766.
Huang, Y., M. Zhang, Y. Xia, Y. Hu, and S. W. Son (2016), Is there a stratospheric radiative feedback in global warming simulations? *Clim. Dyn.*, *46*(1–2), 177–186, doi:10.1007/s00382-015-2577-2.
Keckhut, P., B. M. Funatsu, C. Claud, and A. Hauchecorne (2015), Tidal effects on stratospheric temperature series derived from successive advanced microwave sounding units, *Q. J. R. Meteorol. Soc.*, *141*(687), 477–483, doi:10.1002/qj.2368.
Klaes, K. D., M. Cohen, Y. Buhler, and P. Schlüssel (2007), An introduction to the EUMETSAT polar system, *Bull. Am. Meteorol. Soc.*, *88*(7), 1085.
Knuteson, R. O., et al. (2004a), Atmospheric emitted radiance interferometer. Part I: Instrument design, *J. Atmos. Oceanic Technol.*, *21*(12), 1763–1776.
Knuteson, R. O., et al. (2004b), Atmospheric emitted radiance interferometer. Part II: Instrument performance, *J. Atmos. Oceanic Technol.*, *21*(12), 1777–1789.
Kursinski, E. R., G. A. Hajj, J. T. Schofield, R. P. Linfield, and K. R. Hardy (1997), Observing Earth's atmosphere with radio occultation measurements using the Global Positioning System, *J. Geophys. Res.*, *102*, 23,429–23,465, doi:10.1029/97JD01569.
Ladstädter, F., et al. (2015), Climate intercomparison of GPS radio occultation, RS90/92 radiosondes and GRUAN over 2002 to 2013, *Atmos. Meas. Tech. Discuss.*, *7*, 11,735–11,769, doi:10.5194/amt-8-1819-2015.
Larar, A. M., et al. (2010), IASI spectral radiance validation inter-comparisons: Case study assessment from the JAIVEx field campaign, *Atmos. Chem. Phys.*, *10*(2), 411–430.
Leroy, S., J. Dykema, and J. G. Anderson (2006), Climate benchmarking using GNSS occultation, in *Atmosphere and Climate*, pp. 287–301, Springer, Berlin Heidelberg.
Leroy, S., J. Anderson, J. Dykema, and R. Goody (2008), Testing climate models using thermal infrared spectra, *J. Clim.*, *21*(9), 1863–1875.
Maddy, E. S., and C. D. Barnet (2008), Vertical resolution estimates in version 5 of AIRS operational retrievals, *IEEE Trans. Geosci. Remote Sens.*, *46*, 2375–2384.
Mannucci, A. J., C. O. Ao, T. P. Yunck, L. E. Young, G. A. Hajj, B. A. Iijima, D. Kuang, T. K. Meehan, and S. S. Leroy (2006), Generating climate benchmark atmospheric soundings using GPS occultation data, Proc. SPIE 6301, Atmospheric and Environmental Remote Sensing Data Processing and Utilization II: Perspective on Calibration/Validation Initiatives and Strategies, 630108, doi:10.1117/12.683973.
Mannucci, A. J., et al. (2011), The impact of large scale ionospheric structure on radio occultation retrievals, *Atmos. Meas. Tech.*, *4*(12), 2837–2850, doi:10.5194/amt-4-2837-2011.
McLandress, C., T. G. Shepherd, A. I. Jonsson, T. Von Clarmann, and B. Funke (2015), A method for merging nadir-sounding climate records, with an application to the global-mean stratospheric temperature data sets from SSU and AMSU, *Atmos. Chem. Phys.*, *15*(16), 9271–9284, doi:10.5194/acp-15-9271-2015.
Moncet, J.-L., G. Uymin, A. E. Lipton, and H. E. Snell (2008), Infrared radiance modeling by Optimal Spectral Sampling, *Am. Meteorol. Soc.*, *65*, 3917–3934, doi:10.1175/2008JAS2711.1.
Moncet, J.-L., G. Uymin, P. Liang, and A. Lipton (2015), Fast and accurate radiative transfer in the thermal regime by simultaneous optimal spectral sampling over all channels, *J. Atmos. Sci.*, *72*, 2622–2641, doi:10.1175/JAS-D-14-0190.1.
Nalli, N. R., et al. (2013), Validation of satellite sounder environmental data records: Application to the Cross-track Infrared Microwave Sounder Suite, *J. Geophys. Res. Atmos.*, *118*, 1–16, doi:10.1002/2013JD020436.
Nash, J., and R. Saunders (2015), A review of Stratospheric Sounding Unit radiance observations for climate trends and reanalyses, *Q. J. R. Meteorol. Soc.*, *141*(691), 2103–2113.
Olsen, E., D. Elliot, E. Fetzer, E. Manning, J. Blaisdell, L. Iredell, and J. Susskind (2016), *AIRS/AMSU/HSB Version 6 Data Disclaimer*, Jet Propulsion Lab., California Institute of Technology, Pasadena, Calif.
Pagano, T. S., H. H. Aumann, D. E. Hagan, and K. Overoye (2003), Prelaunch and in-flight radiometric calibration of the Atmospheric Infrared Sounder (AIRS), *IEEE Trans. Geosci. Remote Sens.*, *41*(2), 265–273.
Parkinson, C. L. (2003), Aqua: An Earth-observing satellite mission to examine water and other climate variables, *IEEE Trans. Geosci. Remote Sens.*, *41*(2), 173–183.
Peters, W., et al. (2007), An atmospheric perspective on North American carbon dioxide exchange: CarbonTracker, *Proc. Natl. Acad. Sci. U.S.A.*, *104*(48), 18,925–18,930.
Philipona, R., et al. (2013), Solar and thermal radiation errors on upper-air radiosonde temperature measurements, *J. Atmos. Oceanic Technol.*, *30*(10), 2382–2393.
Revercomb, H. E., H. Buijs, H. B. Howell, D. D. LaPorte, W. L. Smith, and L. A. Sromovsky (1988), Radiometric calibration of IR Fourier transform spectrometers: Solution to a problem with the High-Resolution Interferometer Sounder, *Appl. Opt.*, *27*(15), 3210–3218.
Revercomb, H. E., et al. (2003), Atmospheric Infrared Sounder (AIRS) validation with Scanning-HIS, in *Fourier Transform Spectroscopy, OSA Technical Digest, Optical Society of America*, pp. 3–6, Quebec City.
Rodgers, C. D. (1976), Retrieval of atmospheric temperature and composition from remote measurements of thermal radiation, *Rev. Geophys.*, *14*, 609–624, doi:10.1029/RG014i004p00609.
Rodgers, C. D. (1990), Characterization and error analysis of profiles retrieved from remote sounding measurements, *J. Geophys. Res.*, *95*, 5587–5595, doi:10.1029/JD095iD05p05587.
Rodgers, C. D., and Connor, B. J. (2003), Intercomparison of remote sounding instruments, *J. Geophys. Res.*, *108*(D3), 4116, doi:10.1029/2002JD002299.
Scherllin-Pirscher, B., A. K. Steiner, G. Kirchengast, M. Schwärz, and S. S. Leroy (2017), The power of vertical geolocation of atmospheric profiles from GNSS radio occultation, *J. Geophys. Res. Atmos.*, *122*, 1595–1616, doi:10.1002/2016JD025902.
Seidel, D. J., et al. (2016), Stratospheric temperature changes during the satellite era, *J. Geophys. Res. Atmos.*, *121*, 664–681, doi:10.1002/2015JD024039.
Seidel, D. J., et al. (2011), Stratospheric temperature trends: Our evolving understanding, *Wiley Interdiscip. Rev. Clim. Change*, *2*(4), 592–616.

Simmons, A. J., et al. (2014), Estimating low-frequency variability and trends in atmospheric temperature using ERA-Interim, *Q. J. R. Meteorol. Soc.*, *140*(679), 329–353.
Smith, W. L., H. B. Howell, H. M. Woolf, and H. E. Revercomb (1983), HIS-A satellite instrument to observe temperature and moisture profiles with high vertical resolution, in *5th Conference on Atmospheric Radiation*, vol. 1, pp. 1–9, Am. Meteorol. Soc., Baltimore, Md.
Smith, W. L., et al. (2009), Technical note: Evolution, current capabilities, and future advance in satellite nadir viewing ultra-spectral IR sounding of the lower atmosphere, *Atmos. Chem. Phys.*, *9*(15), 5563–5574.
Steiner, A. K., et al. (2011), GPS radio occultation for climate monitoring and change detection, *Radio Sci.*, *46*, RS0D24, doi:10.1029/2010RS004614.
Steiner, A. K., et al. (2013), Quantification of structural uncertainty in climate data records from GPS radio occultation, *Atmos. Chem. Phys.*, *13*(3), 1469–1484, doi:10.5194/acp-13-1469-2013.
Strow, L. L., S. E. Hannon, M. Weiler, K. Overoye, S. L. Gaiser, and H. H. Aumann (2003a), Prelaunch spectral calibration of the Atmospheric Infrared Sounder (AIRS), *IEEE Trans. Geosci. Remote Sens.*, *41*(2), 274–286.
Strow, L. L., et al. (2003b), An overview of the AIRS radiative transfer model, *IEEE Trans. Geosci. Remote Sens.*, *41*(2), 303–313.
Strow, L. L., et al. (2013), Spectral calibration and validation of the Cross-track Infrared Sounder on the Suomi NPP satellite, *J. Geophys. Res. Atmos.*, *118*, 12,486–12,496, doi:10.1002/2013JD020480.
Sun, B., A. Reale, D. J. Seidel, and D. C. Hunt (2010), Comparing radiosonde and COSMIC atmospheric profile data to quantify differences among radiosonde types and the effects of imperfect collocation on comparison statistics, *J. Geophys. Res.*, *115*, D23104, doi:10.1029/2010JD014457.
Sun, B., A. Reale, S. Schroeder, D. J. Seidel, and B. Ballish (2013), Toward improved corrections for radiation-induced biases in radiosonde temperature observations, *J. Geophys. Res. Atmos.*, *118*, 4231–4243, doi:10.1002/jgrd.50369.
Susskind, J., C. D. Barnet, and J. M. Blaisdell (2003), Retrieval of atmospheric and surface parameters from AIRS/AMSU/HSB data in the presence of clouds, *IEEE Trans. Geosci. Remote Sens.*, *41*(2), 390–409, doi:10.1109/TGRS.2002.808236.
Susskind, J., J. M. Blaisdell, L. Iredell, and F. Keita (2011), Improved temperature sounding and quality control methodology using AIRS/AMSU data: The AIRS science team version 5 retrieval algorithm, *IEEE Trans. Geosci. Remote Sens.*, *49*, 883–907, doi:10.1109/TGRS.2010.2070508.
Syndergaard, S. (2000), On the ionosphere calibration in GPS radio occultation measurements, *Radio Sci.*, *35*, 865–883, doi:10.1029/1999RS002199.
Thompson, D., et al. (2012), The mystery of recent stratospheric temperature trends, *Nature*, *491*(7426), 692–697.
Tobin, D. C., H. E. Revercomb, R. O. Knuteson, B. M. Lesht, L. L. Strow, S. E. Hannon, W. F. Feltz, L. A. Moy, E. J. Fetzer, and T. S. Cress (2006a), Atmospheric Radiation Measurement site atmospheric state best estimates for Atmospheric Infrared Sounder temperature and water vapor retrieval validation, *J. Geophys. Res.*, *111*, D09S14, doi:10.1029/2005JD006103.
Tobin, D. C., H. E. Revercomb, C. C. Moeller, and T. S. Pagano (2006b), Use of atmospheric infrared sounder high-spectral resolution spectra to assess the calibration of moderate resolution imaging spectroradiometer on EOS Aqua, *J. Geophys. Res.*, *111*, D09S05, doi:10.1029/2005JD006095.
Tobin, D. C., et al. (2006c), Radiometric and spectral validation of atmospheric Infrared Sounder observations with the aircraft-based Scanning High-Resolution Interferometer Sounder, *J. Geophys. Res.*, *111*, D09S02, doi:10.1029/2005JD006094.
Tobin, D., et al. (2013), Suomi-NPP CrIS radiometric calibration uncertainty, *J. Geophys. Res. Atmos.*, *118*, 10,589–10,600, doi:10.1002/jgrd.50809.
Tobin, D., R. Holz, F. Nagle, and H. Revercomb (2016), Characterization of the Climate Absolute Radiance and Refractivity Observatory (CLARREO) ability to serve as an infrared satellite intercalibration reference, *J. Geophys. Res. Atmos.*, *121*, 4258–4271, doi:10.1002/2016JD024770.
Wang, L., Y. Han, D. Tremblay, F. Weng, and M. Goldberg (2012a), Inter-comparison of NPP/CrIS radiances with VIIRS, AIRS, and IASI: A post-launch calibration assessment, in Proc. of SPIE, vol. 8528, pp. 85280J-1.
Wang, L., C.-Z. Zou, and H. Qian (2012b), Construction of stratospheric temperature data records from stratospheric sounding units, *J. Clim.*, *25*(8), 2931–2946.
Wee, T.-K., and Y.-H. Kuo (2014), Advanced stratospheric data processing of radio occultation with a variational combination for multifrequency GNSS signals, *J. Geophys. Res. Atmos.*, *119*, 11,011–11,039, doi:10.1002/2014JD022204.
Wielicki, B. A., et al. (2013), Achieving climate change absolute accuracy in orbit, *Bull. Am. Meteorol. Soc.*, *94*(10), 1519–1539.
Young, P. J., et al. (2011), The seasonal cycle and interannual variability in stratospheric temperatures and links to the Brewer-Dobson circulation: An analysis of MSU and SSU data, *J. Clim.*, *24*(23), 6243–6258.
Yulaeva, E., J. R. Holton, and J. M. Wallace (1994), On the cause of the annual cycle in tropical lower-stratospheric temperatures, *J. Atmos. Sci.*, *51*(2), 169–174.
Zou, X., L. Lin, and F. Weng (2014), Absolute calibration of ATMS upper level temperature sounding channels using GPS RO observations, *IEEE Trans. Geosci. Remote Sens.*, *52*(2), 1397–1406.